MICROSCOPIC STUDY OF THE ONSET OF LARGE DEFORMATIONS IN THE ZIRCONIUM REGION

By

SURRINDER KUMAR KHOSA

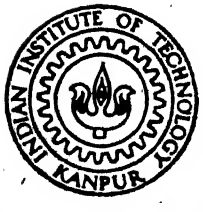

DEPARTMENT OF PHYSICS

INDIAN INSTITUTE OF TECHNOLOGY, KANPUR

AUGUST, 1981

MICROSCOPIC STUDY OF THE ONSET OF LARGE DEFORMATIONS IN THE ZIRCONIUM REGION

A Thesis Submitted
in Partial Fulfilment of the Requirements
for the Degree of
DOCTOR OF PHILOSOPHY

By
SURRINDER KUMAR KHOSA

to the
DEPARTMENT OF PHYSICS
INDIAN INSTITUTE OF TECHNOLOGY, KANPUR
AUGUST, 1981

PHY-1981-D-KHO-MIC

To My Parents

CERTIFICATE

Certified that the work presented in this thesis entitled, "Microscopic Study of the Onset of Large Deformations in the Zirconium Region" by Mr Surrinder Kumar Khosa has been carried out under my supervision and that this has not been submitted elsewhere for a degree.

S.K. Sharma

(S K SHARMA)
Assistant Professor
Department of Physics
Indian Institute of Technology Kanpur
KANPUR-16 (India)

8/4/1992

ACKNOWLEDGEMENTS

At the onset, I would like to thank Dr Satish Kumar Sharma of the Indian Institute of Technology, Kanpur who, despite his very busy schedule, guided me through this thesis. Working with him was truely a learning experience. In the beginning when I was confronted with the problem of selection of the kind of research work I should take up, he brought me out of woods and identified the same for me. During the course of the research work, his timely comments and suggestions were always fruitful and inspiring. I would like to record my debt of gratitude for the amiable and co-operative manner in which he tendered his fruitful assistance and contributions and made himself available whenever approached for the purpose. I am indebted to him not only for much of what has gone into this thesis but also for invoking in me a keen interest in the many-body physics. My special thanks are also due to him for his unabated interest in the problem and the confidence which he reposed in me, inducing in me forbearance so essential in the achievement of this end.

I also want to thank Prof. Y.R. Waghmare to whom I also owe many of the ideas and methods used in this thesis. He made many helpful suggestions and raised many questions that served as guidelines to this work. His friendliness and understanding are also deeply appreciated.

The help rendered by the staff members of the DEC-system 1099, IIT Kanpur, is gratefully acknowledged.

It is also a pleasure to thank my friends Mr P.N. Tripath and Mr T.K. Mani who helped me in the proof reading of the typed stencils.

I am also grateful to Prof. M.K. Khera, the Head of Physics Department, Kashmir University for sparing me for a few months, so as to enable me to complete my work at the Institute.

Finally I should like to thank Mr S L Rathore for skilfully, accurately and quickly transforming the pages of scratched manuscript into these beautifully typed pages. I am also thankful to Mr H K Panda for neatly and skilfully cyclostyling the stencils.

TABLE OF CONTENTS

LIST OF TABLES

LIST OF FIGURES

SYNOPSIS

S K KHOSA
PhD (Physics)
Indian Institute of Technology Kanpur
JULY 1981

"MICROSCOPIC STUDY OF THE ONSET OF LARGE DEFORMATIONS AND SHAPE-COEXISTENCE IN THE ZIRCONIUM REGION"

It is generally felt that the neutron-proton (n-p) effective interactions possess deformation-producing tendency and the neutron-neutron (n-n) or proton-proton (p-p) effective interactions are mostly of the spherifying nature. These ideas have played pivotal roles in the development of the stretch scheme of Danos and Gillet, the roton model of Arima and Gillet and the recent interacting boson model.

The above assumptions regarding the nature of the two components of the effective interactions owe their origin mostly to the fact that the nuclei in the 2s-1d and 2p-1f shells in which both protons and neutrons occupy half-filled sub-shells usually display a number of features associated with well-deformed intrinsic states. On the other hand, the low-lying spectra in the neutron-excess nuclei in these shells are generally marked by an absence of deformation characteristics. Whereas the low-lying levels in ^{20}Ne, ^{44}Ti and ^{60}Zn are quasi-rotational, those in ^{20}O, ^{44}Ca and ^{60}Ni display no analogous deformation trends.

Some time ago a new region of deformation has been discovered around A = 100; well-developed rotational spectra were observed in several highly neutron-rich isotopes of Zirconium and Molybdenum during a study of the fission fragments of ^{252}Cf. The observed B(E2) values were as enhanced as in the rare-earth and the actinide regions.

It is difficult to understand the occurrence of rotational spectra in the Zirconium and Molybdenum isotopes in the framework of the traditional notions concerning the nature of the like-particle effective interactions. The recent observations in the Zirconium region thus call for a careful assessment of the deformation-producing tendency of the n-n (or p-p) channel of the effective interaction.

A Hartree-Fock oriented analysis of the nature of the like-particle part of the two-body interaction is the starting point of the present work. The study provides a qualitative understanding of the occurrence of large deformations in the Zirconium region. This is followed by a microscopic study of number of interesting features associated with the observed quasirotational spectra in the neutron-rich isotopes of Zirconium, Molybdenum and Palladium.

Chapter I presents the background and the genesis of the topics that we have selected for investigation in the present work.

In Chapter II we have given an analysis of the n-p part and the part operative between the like-particles of the

various available effective interactions operative in 2s-1d, 2p-1f and 2p-1f-1g shells, as regards their deformation producing and pairing tendencies. Contrary to the widely-held belief, we found that like-particle interactions have almost the same deformation-producing character as the neutron-proton ones. Deformed Hartree-Fock method has been used for extracting the information concerning the deformation-producing tendency of the interactions. In this connection, we have examined the reliability of the various HF states involved by carrying out second-order perturbative calculations. A significant result that emerges from the present study is the following. It turns out that the relative importance of the pairing effects in the like-particle as well as the neutron-proton channels depends critically on the overall spread of the spherical single particl energies. This interplay of the single-particle energies and the various components of the effective interactions is shown to explain the absence of rotational behaviour in the neutron-excess nuclei in the 2s-1d and 2p-1f shells.

The above analysis of the various parts of the effective interactions proves instrumental in explaining the dramatic emergence of the rotational spectra in the $A > 100$ region. Chapter III presents a systematic study of the onset of large deformations in the highly neutron-rich Zirconium and Molybdenum isotopes. The calculations employ pairing-plus-quadrupole-quadrupole effective interactions operating in a valence space spanned by the $1g_{9/2}$, $2d_{5/2}$, $3s_{1/2}$, $2d_{3/2}$, $1g_{7/2}$ and $1h_{11/2}$

orbits for protons as well as neutrons. The nucleus ^{80}Zr has been considered to be an inert core. The present choice of the large valence space ensures an unbiased study of the deformation effects in this region. The yrast spectra in various cases have been obtained in the framework of the Cranked Hartree-Fock-Bogoliubov approach. A number of interesting observed features in the Zirconium region connected with the dramatic onset of large deformations as well as the coexistence of deformed and spherical intrinsic shapes can be successfully understood in terms of the important roles played by the deformation of ^{94}Sr core and the increased participation of the $1h_{11/2}$ level in the valence space.

A new phenomenon has some time ago been observed in the level schemes of ^{102}Pd and ^{100}Pd populated by heavy-ion induced reactions: the ground state bands of these nuclei reach $J = 14$, but "fork" into two branches, at $J = 8^+$ state in ^{102}Pd and at the $J = 6^+$ state in ^{100}Pd. Further, the ground state bands in these nuclei have been observed to reveal significant departures from the rotational behaviour. Although attempts have been made recently to explain the observed spectra phenomenologically by invoking the "variable-moment of inertia" (VMI) model, microscopic calculations have been lacking. The successful calculation of the yrast spectra in Zr and Mo isotopes encouraged us to make an attempt at explaining the yrast and the yrare spectra in the nuclei $^{100,102}Pd$ employing the $3s-2d-1g-1h_{11/2}$ configuration space,

in conjuction with the pairing-plus-quadrupole-quadrupole effective interaction. The results are discussed in the Chapter IV. Our first-ever microscopic study of Palladium isotopes brought out again the important role played by the $1h_{11/2}$ orbital vis-a-vis the occurrence of forking effect as well as the significant deviations from quasirotational behaviour. Further, in sharp contrast the suggestions made in a couple of phenomenological studies of Pd isotopes in the recent past, it turned out that it is unnecessary to invoke asymmetric deformations in connection with the observed features of the yrast and the yrare spectra in the Palladium isotopes.

CHAPTER I

INTRODUCTION

It is generally found that the nuclei in the 2s-1d and 2p-1f shells, in which both protons and neutrons occupy half-filled sub-shells, display a number of features which are distinctly interpretable in terms of deformed intrinsic states. Nuclei such as ^{20}Ne, ^{24}Mg, ^{44}Ti, ^{52}Fe and ^{60}Zn are some typical examples. On the other hand, the nuclei consisting of only neutrons as valence particles display a conspicuous lack of rotational collectivity. Some examples of this category are provided by the Oxygen isotopes ($^{20,22,24}O$), Calcium isotopes ($^{44-50}Ca$) and Nickel isotopes($^{58-64}Ni$).

An attempt is usually made to rationalize the above-mentioned features by associating the deformation-producing and the pairing tendencies with the neutron-proton (V_{np}) and the like-particle (V_{nn+pp}) effective interactions respectively. In fact these assumptions concerning the two channels of effective interactions are implicit in the formulation of the stretch scheme of Danos and Gillet[1] as well as the roton model of Arima and Gillet[2]. The idea that the neutron-proton interaction is the major source of deformations is also inherent to some degree, in the recent Interacting Boson Model[3].

Recently Cheifetz *et al.*[4] have discovered a new region of deformation around A=100. By studying the fission fragments

of ^{252}Cf, they observed rotational spectra in the nuclei ^{100,102}Zr and ^{102,104,106}Mo. The measured B(E2) values for these nuclei were as enhanced as in the rare-earth and actinide regions.

The assumption that the nucleus ^{90}Zr can be considered "inert", has formed the basis of a large number of reasonably successful shell-model studies[5] in the nuclei with A=91-96. The discovery of the well-developed rotational spectra in the highly neutron-rich Zr isotopes, therefore, appears quite puzzling; it seems very difficult to reconcile the observed onset of large deformations in these isotopes with the traditional pairing caricature of the like-particle interactions.

The recent experimental observations in the Zirconium region thus cast doubts on the correctness of the usual notions which associate the pairing or spherifying character with the like-particle effective interactions. It thus appears worthwhile to carry out an assessment of the deformation-producing role of the like-particle part of the two-body effective interactions operative in the 2s-1d, 2p-1f and 2p-1f-1g shells. This is precisely what we have done in Chapter II, where the Hartree-Fock (HF) method has been employed to glean information about the deformation-producing roles of the interactions V_{np} and V_{nn+pp}. Our calculations differ from those carried out by Nair *et al.*[6] some time ago in that we have made an attempt at delineating the roles played by the spherical single-particle

Hamiltonian. Our results bring out the link between the nature of the spectrum of spherical SPE's and the possibility of an onset of rotational features. We find that the interaction V_{nn+pp} has about the same deformation-producing tendency as the interaction V_{np} and that they both have a dominant quadrupole-quadrupole character. We have also tried to examine, by carrying out second-order perturbative calculations, the connection between the overall spread of the SPE's and the relative importance of the pairing effects in the like-particle as well as the neutron-proton channels.[7] The calculations show that it is erroneous to interpret the absence of rotational features in the neutron-excess nuclei in the 2s-1d and 2p-1f shells in terms of the "pairing" nature of the interaction V_{nn+pp}.

The above analysis of the various parts of the effective interactions proves instrumental in understanding, at least qualitatively, the occurrence of large deformations in the nuclei $^{100,102}Zr$; the significant degeneracy of the relevant spherical SPE's for the A=80-100 nuclei offers the interesting possibility of building up sizable deformations in this region for even those nuclei which possess only neutrons as the valence particles.

Chapter III presents a quantitative study of the onset of large deformations in the highly neutron-rich Zirconium and Molybdenum isotopes. We have employed the Cranked Hartree-Fock-Bogoliubov (CHFB) theory in conjunction with the pairing-

lus-quadrupole-quadrupole effective interactions operating in the valence space spanned by the $2p_{1/2}$, $1g_{9/2}$, $2d_{5/2}$, $3s_{1/2}$, $2d_{3/2}$, $1g_{7/2}$ and $1h_{11/2}$ orbits for protons as well as neutrons. The nucleus ^{80}Zr has been considered to be an inert core. The present choice of the large valence space ensures an unbiased study of the deformation trends in this region.

Federman and Pittel[8-11] have recently conjectured that the dramatic onset of large deformations in the nuclei $^{100,102}Zr$ may be related to the deformation-producing role of the $[(1g_{9/2})_p - (1g_{7/2})_n]$ interactions. Their suggestions imply a correlation between the occurrence of deformations and the simultaneous occupation of the orbits $(1g_{7/2})_n$ and $(1g_{9/2})_p$. Our explicit HFB calculations[12], however, reveal that the interaction of the $1g_{9/2}$-protons with the $1g_{7/2}$-neutrons plays very little role. We find that the involvement of the $1h_{11/2}$ orbit is one of the major factors governing the intrinsic quadrupole deformations in the nuclei $^{100,102}Zr$ and $^{102,104,106}Mo$.

Recently an attempt was made by Federman, Pittel and Campos[10] to examine the co-existence of the spherical as well as deformed shapes in the Zirconium region by carrying out shell-model studies of some of the lighter Zr isotopes ($94<A<100$). Their calculations involved an inert ^{94}Sr core with the protons confined to the orbits ($2p_{1/2}$, $1g_{9/2}$, $2d_{5/2}$) and the neutrons to the orbits ($3s_{1/2}$, $2d_{3/2}$, $1g_{7/2}$, $1h_{11/2}$). Our CHFB calculations however reveal that the

ccurrence of deformed intrinsic shapes in the Zirconium and olybdenum isotopes with A>100 is not compatible with the ssumption of an inert ^{94}Sr core. The yrast spectra that we ıave obtained for the nuclei ^{100,102}Zr and ^{104,106}Mo by :mploying the usual Cranked Hartree-Fock-Bogoliubov (CHFB) :echnique[13,14] are in reasonable agreement with the experiments.

Scharff-Goldhaber et al.[15] have some time ago reported on the level schemes of the nuclei ^{100}Pd (N=54, Z=46) and ^{102}Pd populated by heavy-ion induced reactions. An important feature that characterizes the yrast (as well as the yrare) spectra in these isotopes is the significant departure from rotational behaviour. Further, the ground state bands of these nuclei reach J=14, but "fork" into two branches, at $J^{\pi}=8^{+}$ in ^{102}Pd and at J=6 in ^{100}Pd.

Although a couple of phenomenological studies have been made some time ago to explain the observed spectra in ^{100,102}Pd, a lack of any explicit microscopic calculation has prevented a clear understanding of the observed features. The "variable moment of inertia" (VMI) model[16] has been partially successful in explaining the observed deviations from the J(J+1) law in the Palladium isotopes. Further, Smith and Volkov[17] have invoked the instability of the symmetric deformed nuclei towards asymmetric deformations in order to explain phenomenologically the forking effect.

The successful quantitative study of the yrast spectra in the doubly even Zr and Mo isotopes encouraged us to make an

ttempt at providing a microscopic understanding of the yrast nd the yrare spectra in the Pd isotopes by carrying out the ariation-after-projection (VAP) calculations[18] with the HFB nsatz for the intrinsic wavefunction. Here again we employ he pairing-plus-quadrupole-quadrupole effective interaction perating in the 3s-2d-1g-$1h_{11/2}$ configuration space. Although oth the CHFB and the VAP procedures allow for the possibility f having different intrinsic state for each yrast level, the alculations of the intra-band electromagnetic transition robabilities are easier to carry out if one employs the latter nethod.

Our VAP results presented in Chapter IV for the nuclei ^{100,102}Pd reveal a somewhat dichotomic character of the yrast spectra in these nuclei; we observe a sudden change of the intrinsic state in going from the yrast $J^{+}=4$ to $J^{+}=6$. The calculation is successful in reproducing to a large extent, the observed deviations from the $J(J+1)$-law.

The microscopic study of the Palladium isotopes that we present in Chapter IV brings out the important role played by the $1h_{11/2}$ orbit vis-a-vis the significant departure of the yrast band from the quasirotational behaviour as well as the appearance of the yrare levels with $J \geq 6$ at low excitation energies. Further, in contrast with the earlier phenomenological studies[17], it turns out that it is not necessary to invoke asymmetric deformations in connection with the yrast and yrare spectra in Palladium isotopes.

Finally, in Chapter V we summarize the results btained in, and wisdom gained from Chapters II, III nd IV.

REFERENCES

1. M. Danos and V. Gillet, Phys. Rev. 161 (1967) 1034.
2. A. Arima and V. Gillet, Ann. Phys. (NY) 66 (1971) 117.
3. F. Iachello, Interacting Bosons in Nuclear Physics, edited by F. Iachello, Plenum Press (New York and London, 1979).
4. E. Cheifetz, R.C. Jared, S.G. Thompson and J.B. Wilhelmy, Phys. Rev. Lett. 25 (1978) 38.
5. J.D. Vergados and T.T.S. Kuo, Phys. Lett. 35B (1971) 93.
6. S.C.K. Nair, A. Ansari and L. Satpathy, Phys. Lett. 71B (1977) 257.
7. S.K. Khosa and S.K. Sharma, to be published in the Physical Review C.
8. P. Federman and S. Pittel, Phys. Lett. 69B (1977) 385.
9. P. Federman and S. Pittel, Phys. Lett. 77B (1978) 29.
10. P. Federman, S. Pittel and R. Campos, Phys. Lett. 82B (1979) 9.
11. P. Federman and S. Pittel, Phys. Rev. C20 (1979) 820.
12. S.K. Khosa, P.N. Tripathi and S.K. Sharma, to be published.
13. H.J. Mang, Phys. Reports 18C (1975) 325.
14. A.L. Goodman, in :Advances in Nuclear Physics, Volume 11, Plenum Press, New York (1979).
15. G. Scharff-Goldhaber, M. McKeown, A.H. Lumpkin and W.F. Piel Jr, Phys. Lett. 44B (1973) 416.
16. M.A.J. Mariscotti, G. Scharff-Goldhaber and B. Buck, Phys. Rev. 178 (1969) 1864.
17. B.C. Smith and A.B. Volkov, Phys. Lett. 47B (1973) 193.
18. L. Satpathy and S.C.K. Nair, Phys. Lett. 26B (1968) 257; R. Dreizler, P. Federman, B. Giraud and E. Osnes, Nucl. Phys. A113 (1968) 145; J. Vojtik, Nucl. Phys. A212 (1973) 138;

CHAPTER II

DEFORMATION-PRODUCING TENDENCY OF THE LIKE-PARTICLE EFFECTIVE INTERACTIONS IN NUCLEI

II.1 Introduction

The nuclei in the 2s-1d and 2p-1f shells in which both protons and neutrons occupy half-filled sub-shells, usually display a number of features associated with well-deformed intrinsic states. On the other hand, the low-lying spectra in the neutron-excess nuclei in these shells are generally marked by an absence of deformation characteristics. Whereas the low-lying levels in ^{20}Ne, ^{44}Ti and ^{60}Zn are quasirotational, those in ^{20}O, ^{44}Ca and ^{60}Ni display no analogous deformation trends.

As mentioned in the preceding chapter, the above observations have led to a feeling that the neutron-proton (n-p) effective interactions possess deformation-producing tendency and the neutron-neutron (n-n) or proton-proton (p-p) effective interactions are mostly of the spherifying nature[1-6]. These ideas have played a pivotal role in the development of the stretch scheme[4] of Danos and Gillet, the roton model[5] of Arima and Gillet and the recent interacting Boson model[6] of Arima *et al.*

Some time ago, Cheifetz *et al.*[7] have observed well-developed rotational spectra in several highly neutron-rich Zr isotopes during a study of fission fragments of ^{252}Cf. The observed

B(E2) values were as enhanced as in the rare-earth and actinide regions. It appears difficult to reconcile the observed dramatic onset of large deformations in the singly closed shell nuclei ^{100,102}Zr with the customary notion of "pairing" type n-n interactions. The observations in the Zr region thus call for a careful assessment of the deformation-producing tendency of the n-p as well as the n-n (or p-p) channels of the effective interactions.

The deformation- or the field-producing character of a given two-body interaction (or a part of it) can quite unambiguously be examined by carrying out a Hartree-Fock (HF) calculation and by comparing the quadrupole moments of the resulting stable HF wave functions with the relevant SU3 or the asymptotic Nilsson model predictions. This is precisely what we have done for some nuclei in the mass range A = 20-80 by employing various realistic effective interactions operative in the 2s-1d, 2p-1f and 2p-1f-1g shells.

An analysis of the deformation-producing tendencies of the T = 0 and T = 1 interactions by Sharma and Bhatt[8,9] had earlier revealed that these components have almost the same behaviour. The n-p interaction has, of course, <u>both</u> T = 0 and T = 1 parts. The like-particle interactions, on the other hand, constitute <u>only</u> a part of the full T = 1 interaction for systems with neutrons as well as protons. Therefore, it is not possible to glean information about the deforming nature of the n-n (or p-p) and n-p components from the earlier work.

In section II.2 we give a brief outline of the deformed Hartree-Fock (HF) method. In section II.3 we present the method for computing the two-particle two-hole (2p-2h) admixtures to the HF state in the framework of second-order perturbation theory. In section II.4 we discuss the results obtained by carrying out deformed HF calculations by employing the different components of the two-body interaction. The significance of the comparison of the intrinsic quadrupole moments extracted from the two-body interactions (through the HF procedure) with the relevant SU3 values is pointed out. Our results show that, in contrast to the general belief, the like-particle component of the effective interaction possesses essentially the same deformation-producing character as the n-p component. Further, a comparison of the computed $\langle Q_o^2 \rangle$ moments with the SU3 values shows clearly the dominant quadrupole-quadrupole ($q^2.q^2$) character of the various effective interactions that we have employed.

Section II.5 contains a discussion of the stability of the various HF minima involved in terms of the quantitative estimates of the 2p-2h admixtures.

The results presented in section II.6 bring out the important role played by the spectrum of the spherical single-particle energies (SPE's) vis-á-vis the relative importance of pairing effects in the like-particle and the neutron-proton channel. It turns out that the general absence of rotational features in the nuclei such as ^{20}O, ^{44}Ca and ^{60}Ni is not so much a reflection of the spherifying nature of the like-particle

interactions, it is just due to the effect of the significantly non-degenerate SPE's.

It is easy to understand, at least qualitatively, the occurrence of large deformations in the Zirconium region in terms of the roles played by the spherical SPE's. This is discussed in section II.7. Section II.8 contains some concluding remarks.

II.2 The Deformed Hartree-Fock Method

Theoretical discussions of the deformations in nuclei are usually based on the unified model of Bohr and Mottelson[10] in which single particle and collective rotational motions are distinguished and uncoupled. In this model, e.g., the state of spin J belonging to the ground-state rotational band of an even-even nucleus is described by the product wave function

$$|JM\rangle = \sqrt{\frac{2J+1}{8\pi^2}}\ D^J_{M0}(\Omega)\ |\phi_0\rangle \qquad J = 0,2,4,\ldots \qquad \text{(II.2.1)}$$

The rotational motion is described by the symmetric top wave function

$$D^J_{M0}(\Omega) = \sqrt{\frac{4\pi}{2J+1}}\ Y^J_M\ (\beta\gamma) \qquad \text{(II.2.2)}$$

The single-particle motion is described by the intrinsic state $|\phi_0\rangle$. The wave function of the nucleus is only expected to factorize when the particle excitation energy or the spacing of intrinsic states is larger than the energy of collective excitation or level spacing in a rotational band. The conditions

are sometimes met in even-even N=Z nuclei in the A=20-60 mass region.

The simplest assumption that can be made about the intrinsic state $|\phi>$ is that it is a Slater determinant of single nucleon orbits in a deformed field.

$$|\phi> = b^+_{\lambda_1} \; b^+_{\lambda_2} \; \ldots \; b^+_{\lambda_A} \; |0> \qquad \text{(II.2.3)}$$

The notation of second quantization is used here, and b^+_λ is the fermion operator which creates a particle in the orbit λ. It obeys the anti-commutation rules

$$[b_\lambda, \; b^+_\mu]_+ = \delta_{\lambda\mu}, [b_\lambda, \; b_\mu]_+ = 0 \qquad \text{(II.2.4)}$$

The purpose of the HF theory is to determine the wave functions of the orbits λ of the Slater determinant (II.2.3). This is achieved by requiring the energy of the system described by the wave function in eq. (II.2.3) to be stationary and minimum for infinitesimal variations of the orbits λ. The energy of the system is obtained by taking the expectation value of the Hamiltonian H in the state of eq. (II.2.3). The Hamiltonian $\hat{H}$ is defined

$$\hat{H} = \sum_{i=1}^{A} \frac{P_i^2}{2m} + \frac{1}{2} \sum_{i \neq j} V(ij) \qquad \text{(II.2.5)}$$

$$E_{HF} = <\phi|H|\phi> = \sum_{\lambda=1}^{A} <\lambda|t|\lambda> + \frac{1}{2} \sum_{\lambda\mu=1}^{A} <\lambda\mu|V|\lambda\mu> \qquad \text{(II.2.6)}$$

where E_{HF} is called the HF energy;

$\langle\lambda|t|\lambda\rangle$ is the kinetic energy of the orbit λ,

and

$$\langle\lambda\mu|V|\lambda\mu\rangle = -\langle\lambda\mu|V|\mu\lambda\rangle \qquad \text{(II.2.7)}$$

is an antisymmetrized matrix element of the two-body interaction $V(ij)$.

It is advantageous to expand the orbits on a basis $|jm\rangle$ of known wave functions

$$|\lambda\rangle = \sum_j C^{\lambda}_{jm}|jm\rangle \qquad \text{(II.2.8)}$$

The basis j may be e.g., the set $|nljm\tau\rangle$ of shell model states in a harmonic oscillator. Any basis may be used to expand the orbits, provided one is able to calculate matrix elements of the interaction V with the basis states. The set of orbits λ (both filled and empty) is assumed to form an orthonormal set of wave functions

$$\sum_j C^{\lambda^*}_{jm} C_{jm}^{\lambda'} = \delta_{\lambda\lambda'}, \sum_{\lambda} C^{\lambda^*}_{jm} C^{\lambda}_{j'm'} = \delta_{jj'}\,\delta_{mm'} \qquad \text{(II.2.9)}$$

The wave function $|\phi\rangle$ is determined by the coefficients C^{λ}_{jm}, which become variational parameters. The energy will be stationary with the normalization condition (II.2.9) when

$$\frac{\partial}{\partial C^{\lambda^*}_{jm}}\left[\langle\phi|H|\phi\rangle - e_\lambda \sum_{jm} C^{\lambda^*}_{jm} C^{\lambda}_{jm}\right] = 0 \qquad \text{(II.2.10)}$$

Here e_λ is introduced as a Lagrange multiplier. With the help of expansion (II.2.8) of the orbits, the energy $\langle\phi|H|\phi\rangle$ in eq.(II.2.10) may be expressed in terms of the known matrix elements of t and V in the known basis $|jm\rangle$. The derivative

(II.2.10) may then be calculated directly, and one obtains

$$\sum_{j'm'} \Big[\langle jm|t|j'm'\rangle + \sum_{\lambda=1}^{A} \sum_{j_1m_1} \sum_{j_2m_2} C^{\lambda *}_{j_1m_1} \langle jm, j_1m_1|V|j'm', j_2m_2\rangle \times C^{\lambda}_{j_2m_2} \Big] C^{\lambda}_{j'm'} = e_\lambda C^{\lambda}_{jm} \qquad \text{(II.2.11)}$$

eqs. (II.2.11) have the form of an eigenvalue problem

$$\sum_{j'm'} \langle jm|h|j'm'\rangle C^{\lambda}_{j'm'} = e_\lambda C^{\lambda}_{jm} \qquad \text{(II.2.12)}$$

where h is a Hamiltonian given by its matrix elements

$$\langle jm|h|j'm'\rangle = \langle jm|t|j'm'\rangle + \sum_{\lambda=1}^{A} \langle jm,\lambda| V |j'm',\lambda\rangle$$

$$= \langle jm|t|j'm'\rangle + \sum_{\lambda=1}^{A} \sum_{j_1m_1} \sum_{j_2m_2} C^{\lambda *}_{j_1m_1} \langle jm, j_1m_1|V|j'm', j_2m_2\rangle C^{\lambda}_{j_2m_2} \qquad \text{(II.2.13)}$$

where h is the HF single particle Hamiltonian. Equations (II.2.12) and (II.2.13) are the HF equations for the orbits λ. They may be solved by the following iteration procedure:[11]

(a) An initial set of coefficients C^{λ}_{jm} is guessed, and also which orbits are occupied.

(b) With this set of coefficients C^{λ}_{jm} the matrix elements of eq. (II.2.13) of the HF Hamiltonian are calculated.

(c) Equation (II.2.12) is solved by diagonalizing the Hamiltonian matrix (II.2.13). A new set of coefficients C^{λ}_{jm} is obtained, and A orbits are chosen to be filled by nucleons. One returns to step (b). This process is repeated until successive diagonalizations produce the same set of coefficients C^{λ}_{jm}.

The iteration procedure is somewhat complicated by the fact that there are many local minima of the energy (II.2.6) and therefore many solutions of the HF equations. Various minima may be reached by various initial guesses, which therefore become crucial. Furthermore, after each diagonalization of the Hamiltonian matrix (II.2.13) one must decide which orbits to fill and it will be seen that the energies of the orbits vary from one solution to another.

In our calculations the starting wave functions have been generated from the deformed single-particle Hamiltonian

$$h = \epsilon_j \delta_{jj'} + \delta q_o^2 \qquad \text{(II.2.14)}$$

We have tried to reduce the time involved in the calculations by storing all possible uncoupled matrix elements of the type $\langle j_1 m_1, j_2 m_2 | V | j_3 m_3, j_4 m_4 \rangle$ which are compatible with the axial symmetry of the orbits $|\lambda\rangle$.

II.3. Calculation of the Second-Order Admixtures to the HF state

The lowest-order correction to the HF intrinsic state ψ_{HF} will be through the admixture of 2p-2h type excited configurations to it. The 2p-2h configurations are limited to the HF single particle states of a given major shell. For the intrinsic HF state $|\phi\rangle$ a typical $|2p\text{-}2h\rangle$ configuration is given by

$$|2p\text{-}2h\rangle = b^+_{\mu_1} b^+_{\mu_2} b_{\lambda_1} b_{\lambda_2} |\phi\rangle \qquad \text{(II.3.1)}$$

The matrix element connecting the Hamiltonian (II.2.5) with a 2p-2h configuration is then given by

$$<2p\text{-}2h|H|\phi> = <\mu_1\mu_2|V|\lambda_1\lambda_2> \qquad (II.3.2)$$

Here μ_1 and μ_2 denote HF empty orbits belonging to the same major shell as the occupied orbits λ_1 and λ_2.

The second order perturbation theory yields the following corrections for the HF-energy and the mass quadrupole moment.

$$\Delta E = - \sum_{\mu_1<\mu_2} \sum_{\lambda_1<\lambda_2} A_{\mu_1\mu_2\lambda_1\lambda_2} <\mu_1\mu_2|V|\lambda_1\lambda_2> \qquad (II.3.3)$$

$$\Delta Q = - (1 + C^2_{2p-2h})^{-1} \sum_{\mu_1<\mu_2} (A_{\mu_1\mu_2\lambda_1\lambda_2})^2$$

$$x\ (q_{\mu_1\mu_1} + q_{\mu_2\mu_2} - q_{\lambda_1\lambda_1} - q_{\lambda_2\lambda_2}) \qquad (II.3.4)$$

The total wave function can be written as

$$\psi = \sqrt{(1 - C^2_{2p-2h})}\ \psi_{HF} + C_{2p-2h}\ \psi_{2p-2h} \qquad (II.3.5)$$

where we have

$$C_{2p-2h} = \frac{C'_{2p-2h}}{\sqrt{(1+C'^2_{2p-2h})}}$$

$$C'_{2p-2h} = \left(\sum_{\mu_1<\mu_2} \sum_{\lambda_1<\lambda_2} A_{\mu_1\mu_2\ \lambda_1\lambda_2}\right)^{\frac{1}{2}} \qquad (II.3.6)$$

The amplitude $A_{\mu_1\mu_2\ \lambda_1\lambda_2}$ is given by

$$A_{\mu_1\mu_2\ \lambda_1\lambda_2} = \frac{<\mu_1\mu_2|V|\lambda_1\lambda_2>_A}{(e_{\mu_1}+e_{\mu_2}-e_{\lambda_1}-e_{\lambda_2})} \qquad (II.3.7)$$

Here $<\mu_1\mu_2|V|\lambda_1\lambda_2>_A$ is an antisymmetrized matrix element. In eq. (II.3.4) the cross terms of the quadrupole operator between various 2p-2h configurations built on the HF-state have been neglected as their effect is expected to be very small. The matrix element of the quadrupole operator between the single

particle states λ_1 and λ_2 is denoted by $q_{\lambda_1 \lambda_2}$.

The squared amplitude $C^2_{2p-2h} = \langle\psi|\psi_{2p-2h}\rangle^2$ expresses the total intensity of the 2p-2h admixtures to the HF intrinsic states.

II.4 Deformation-producing Tendency of the Like-particle Effective Interactions In The 2s-1d, 2p-1f and 2p-1f-1g shells

In order to assess the deformation or the field producing character of the parts V_{nn} and V_{nn+pp} of various effective interactions operative in the 2s-1d, 2p-1f and 2p-1f-1g shells, we have carried out deformed HF calculations and compared the intrinsic quadrupole moments of the stable HF minima with the relevant SU3 or the asymptotic Nilsson model predictions.

In Table II.1(a) we first present the results obtained in the case of the nucleus ^{20}Ne. The valence space is spanned by the $1d_{5/2}$, $2s_{1/2}$ and $1d_{3/2}$ orbits. The nucleus ^{16}O is treated as an inert core. The relevant effective two-body interaction that we have employed is a renormalized G matrix due to Kuo[12] which is a sum of G_{bare} and G_{3p-1h} in the ^{16}O core. The Kuo interaction has earlier been employed by Halbert[13] et al. in a large number of successful shell-model calculations in the 2s-1d shell. The one-body part of the Hamiltonian is specified by the observed ^{17}O energies (in MeV) : $\varepsilon(2s_{\frac{1}{2}}) = 0.87$, $\varepsilon(1d_{5/2}) = 0.0$ and $\varepsilon(1d_{3/2}) = 5.08$. We compare here the quadrupole moments of the HF states resulting from

TABLE II.1

The HF energies (E), intrinsic quadrupole moments $\langle Q_o^2 \rangle$ and the energy gaps (G) of the HF states of ^{20}Ne obtained with different components (V) of the effective interaction. The quadrupole moments are given in units of b^2, where b is the harmonic oscillator parameter. The SU_3 value for the quadrupole moment of ^{20}Ne is 16.0 b^2. The last two columns summarize the results of the second-order perturbation calculation.

V	E(MeV)	$\langle Q_o^2 \rangle$	G(MeV)	ΔE_{2p-2h}	C^2_{2p-2h}(%)
		(a) Experimental SPE's			
Full	-37.80	15.45	7.25	-0.18	00.95
V_{nn+pp}	-20.45	13.76	1.15	-1.08	20.37
V_{np}	-31.20	15.16	4.89	-0.66	04.76
		(b) Degenerate SPE's			
Full	-26.57	15.58	8.44	-0.15	00.79
V_{nn+pp}	-7.26	15.61	2.31	-0.49	08.44
V_{np}	-19.30	15.60	6.12	-0.74	05.36

(i) the full Kuo interaction

(ii) only the like-particle (n-n and p-p) part (labelled as V_{nn+pp}) of the interaction, with the n-p part set equal to zero, and

(iii) only the n-p part (labelled as V_{np}) of the interaction with the like-particle part set equal to zero.

It may be noted here that the calculations (ii) and (iii) violate isospin invariance. The main aim of our model calculations is to isolate the deformation-producing tendency of the V_{nn+pp} and V_{np} parts of the effective interactions. The results are not intended for comparison with any real data. Hence the violation of a well-established symmetry is not objectionable.

It is seen that the quadrupole deformation $\langle Q_0^2 \rangle$ of the HF state resulting from the full interaction is 15.45 b^2, where b ($=\sqrt{\hbar/M\omega}$) is the harmonic oscillator parameter. When <u>only</u> the like-particle interactions are employed, the quadrupole deformation is 13.76 b^2, whereas n-p interaction <u>alone</u> yields $\langle Q_0^2 \rangle = 15.16\ b^2$. We thus find here that the n-p interactions yield only <u>slightly</u> more quadrupole deformation than the like-particle ones.

With a given spectrum of the spherical SPE's the quadrupole deformations of the HF wave function depends not only on the <u>multipole character</u> of the interaction but also on its <u>strength</u>. We therefore switch off the SPE's because our primary aim here is to isolate and compare the deformation-producing tendencies

of the n-p and the like-particle interactions. With the one-body part of the Hamiltonian absent, the wave functions (and hence the deformations) become independent of the strength of the interaction. The HF energy then depends linearly on the interaction strength.

The results obtained with the degenerate SPE's (Table II.1(b)) reveal quite dramatically the identical deforming tendencies of the n-p and the like-particle interactions; whereas the full interaction yields $\langle Q_o^2 \rangle = 15.58\ b^2$, the intrinsic quadrupole moments of the HF states resulting from the like-particle interactions and the n-p interactions are $15.61\ b^2$ and $15.60\ b^2$ respectively.

Note also that the HF energy resulting from the full interaction is almost the sum of the energies obtained in the case of the interactions V_{nn+pp} and V_{np}. This again implies that the deformed HF wave functions obtained from the three interactions (viz. V_{nn+pp}, V_{np} and the full interaction) are nearly identical.

The magnitude of the intrinsic $\langle Q_o^2 \rangle$ moments resulting from V_{nn+pp} and V_{np} are quite close to the SU3 values. To appreciate the significance of this result we first note that the HF self-consistent single-particle field obtained from a two-body interaction V can be written as

$$V_{H-F} = \sum_{\alpha\beta} \{ \sum_{\gamma\delta} V_{\alpha\gamma\beta\delta} \langle a_\gamma^+ a_\delta \rangle \} a_\alpha^+ a_\beta .$$

(Here the expectation values $\langle \ldots\ldots \rangle$ are taken with respect to the HF state).

Assuming the potential $V = V_o \sum_{i<j} q(i).q(j)$ and neglecting the exchange term (the Hartree approximation) we get

$$V_H = \sum_{\alpha\beta} \{ V_o \sum_{\mu} (-1)^{\mu} \sum_{\gamma\delta} \langle\alpha|q_{\mu}|\beta\rangle\langle\gamma|q_{-\mu}|\delta\rangle \langle a_{\gamma}^{+} a_{\delta}\rangle\} a_{\alpha}^{+} a_{\beta}.$$

Since $q_{\mu} = \sum_{\alpha\beta} \langle\alpha|q_{\mu}|\beta\rangle a_{\alpha}^{+} a_{\beta}$, V_H can be recast in the form

$$V_H = V_o \sum_{\mu} (-1)^{\mu} \langle q_{-\mu}\rangle q_{\mu}$$

If we assume[14] that an axially symmetric, SU3 intrinsic state $\phi(\lambda o)$ of maximum weight has been employed in the r.h.s. of the above equation, then V_H becomes proportional to q_o. Thus, within the Hartree approximation, the self-consistent intrinsic states resulting from a pure q.q two-body interaction is just the SU3 state of maximum weight. In view of this result, the closeness of our computed $\langle Q_o^2\rangle$ values to the relevant SU3 values clearly implies the dominant q.q character of the three sets of interactions employed, viz., the complete Kuo interaction, its n-p part and the part operative between the like particles.

The validity of the above conclusions depends very much on the reliability of the HF wave functions involved. We shall return to the problem of assessing the goodness of the HF states later in the section II.5.

Next we present in Table II.2 and II.3 the results obtained for some nuclei in the 2p-1f and 2p-1f-1g shells. The calculations for the nuclei ^{44,48}Ti, ^{48,52}Cr and ^{56,62}Ni have been carried out by using the renormalized interaction, $(G + G_{3p1h})$, obtained by Kuo and Brown[15] for the valence space consisting of

TABLE II.2

The HF energies as well as the intrinsic quadrupole moments for some nuclei in the 2p-1f shell. The spherical SPE's have been taken to be degenerate.

	Nucleus	Interaction	E(in MeV)	$\langle Q_o^2 \rangle$	$\langle Q_o^2 \rangle_{SU3}$
		Full	-16.42	23.24	
(a)	$^{44}_{22}Ti_{22}$	$V_{nn}+V_{pp}$	-4.64	23.28	24.00
		V_{np}	-11.77	23.30	
		Full	-30.99	35.37	
(b)	$^{48}_{22}Ti_{26}$	$V_{nn}+V_{pp}$	-11.03	35.39	36.00
		V_{np}	-20.00	35.23	
		Full	-35.84	35.32	
(c)	$^{48}_{24}Cr_{24}$	$V_{nn}+V_{pp}$	-9.93	35.09	36.00
		V_{np}	-25.95	35.64	
		Full	-57.34	41.57	
(d)	$^{52}_{24}Cr_{28}$	$V_{nn}+V_{pp}$	-16.33	41.47	42.00
		V_{np}	-41.09	41.46	
		Full	-94.68	47.79	
(e)	$^{56}_{28}Ni_{28}$	$V_{nn}+V_{pp}$	-22.73	47.81	48.00
		V_{np}	-71.95	47.79	
		Full	-127.08	41.92	
(f)	$^{62}_{28}Ni_{34}$	$V_{nn}+V_{pp}$	-29.28	41.82	42.00
		V_{np}	-98.41	41.02	

TABLE II.3.

The HF energies as well as the intrinsic quadrupole moments for some nuclei in the 2p-1f-1g shell. All the spherical SPE's are degenerate.

	Nucleus	Interaction	E	$\langle Q_o^2 \rangle$	$\langle Q_o^2 \rangle_{max}$
		Full	-9.34	20.13	
(a)	$^{60}_{30}Zn_{30}$	$V_{nn}+V_{pp}$	-2.42	20.14	20.24
		V_{np}	-6.92	20.14	
		Full	-26.87	32.01	
(b)	$^{66}_{30}Zn_{36}$	$V_{nn}+V_{pp}$	-10.13	29.91	32.36
		V_{np}	-17.89	31.84	
		Full	-26.99	29.69	
(c)	$^{64}_{32}Ge_{32}$	$V_{nn}+V_{pp}$	-7.70	29.23	30.88
		V_{np}	-19.33	29.94	
		Full	-61.26	34.04	
(d)	$^{74}_{32}Ge_{42}$	$V_{nn}+V_{pp}$	-19.90	37.43	38.48
		V_{np}	-44.17	33.74	
		Full	-47.34	36.98	
(e)	$^{68}_{34}Se_{34}$	$V_{nn}+V_{pp}$	-13.10	36.32	38.88
		V_{np}	-34.30	37.34	
		Full	-82.54	39.12	
(f)	$^{76}_{34}Se_{42}$	$V_{nn}+V_{pp}$	-22.61	40.96	42.48
		V_{np}	-61.65	38.90	

the orbits $1f_{7/2}$, $2p_{3/2}$, $2p_{1/2}$ and $1f_{5/2}$. The nucleus ^{40}Ca is considered as an inert core and the one-body part of the Hamiltonian is defined by the observed ^{41}Ca spectrum: (in MeV) $\varepsilon(1f_{7/2})=0.0$, $\varepsilon(2p_{3/2})=2.1$, $\varepsilon(2p_{1/2})=3.9$ and $\varepsilon(1f_{5/2}) = 6.5$. The calculations for the nuclei $^{60,66}Zn$, $^{64,74}Ge$ and $^{68,76}Se$ have been carried out by choosing the valence space spanned by the $2p_{3/2}$, $1f_{5/2}$, $2p_{1/2}$ and $1g_{9/2}$ orbits. The interaction that we use is a sum of G_{bare}, G_{3p-1h} and G_{2p-2h} calculated by Kuo[16] for the ^{56}Ni core. The experimental SPE's, taken from ^{57}Ni spectrum, are (in MeV): $\varepsilon(2p_{3/2}) = 0.0$, $\varepsilon(2p_{1/2}) = 1.08$, $\varepsilon(1f_{5/2}) = 0.78$ and $\varepsilon(1g_{9/2}) = 3.0$.

The minimum-energy HF states for the nuclei considered here possess axial symmetry. The striking similarity of the deformation-producing tendencies of the like-particle and the n-p interactions again manifests itself here in the (almost) identical $\langle Q_0^2 \rangle$ values resulting from these interactions for various nuclei. Further, the HF quadrupole moments obtained from the n-p as well as the like-particle interactions are again almost the maximum possible ones for all the nuclei considered here, reflecting the dominant q.q character of the two components of the effective interaction.

II.5 Stability Of The Hartree-Fock Solutions

The stability of the HF minima depends in a critical manner on the competition between the magnitude of the energy gap (G) at the Fermi surface and the strength of the interaction.

Usually an energy gap of about 2 MeV or more can be regarded safe enough to check the onset of pairing correlations in the HFB framework, in the 2s-1d or 2p-1f shell. From the results presented in column 4, Table II.1, one notes that this is indeed so, except in one case when we employ (V_{nn+pp}) in the presence of the experimental single-particle energies.

We have also examined quantitatively the goodness of the HF states by computing <u>all</u> possible 2p-2h admixtures to them, in the framework of second-order perturbation theory. It should be mentioned here that the Kuo interaction employed in the present work has already been partially renormalized by ^{16}O core polarization processes. These processes cannot be described within the 2s-1d space. The 2p-2h states considered here correspond to the excitations from the occupied 2s-1d shell HF orbitals to the unoccupied 2s-1d shell orbitals. In columns 5 and 6, Table II.1, we give the lowering of the HF energies (ΔE), as well as the total intensity, $C^2_{2p-2h} (= \sum_{2p2h} \langle\psi| \psi_{2p2h}\rangle^2)$, of the various 2p-2h admixtures.

We first consider here the results obtained in the case (b) when the SPE's are degenerate. In view of the smallness of the corrections obtained here, the HF wave functions obtained in various cases for the nucleus ^{20}Ne can be expected to provide a reasonably good approximation to the relevant exact shell model wave functions.

From the results obtained in the presence of the experimental SPE's (case a), we find that whereas the admixtures resulting

from V_{nn+pp} are about 20.4 percent, those due to V_{np} are only about 4.8 percent. As we shall see in the next section, this result is not confined to the present case alone; it is connected with the role of the spherical SPE's in giving rise to enhanced pairing effects in the neutron-excess nuclei in the 2s-1d, 2p-1f and 2p-1f-1g shells.

From the results of the perturbation calculation for some of the axially symmetric nuclei in the 2p-1f and 2p-1f-1g shells (see columns 9-12, Table II.4(a)) we note that various HF states obtained here can also be considered fairly reliable; the total intensity of all possible 2p-2h corrections is always less than 21 percent. It may be mentioned that the usual 2p-2h correlations involved in an HFB type calculation are only a small fraction of the total admixtures considered here - whereas one excites only time-reversed, K=0 pairs in the HFB scheme, we have included both K=0 as well as K≠0 pairs.

II.6 Role of the Spherical SPE's vis-á-vis the Enhanced Pairing Effects in the Like-particle Channel

We now turn to the question of the general absence of rotational collectivity in the neutron-excess nuclei in A=16-60 region. In Table II.4(b) we present the results obtained in the case of the nuclei ^{44,48}Ti and ^{60}Zn by employing the relevant SPE's for the 2p-1f and 2p-1f-1g shells. A comparison of these results with those presented in Table II.4(a) brings out dramatically the role of the experimental SPE's in these shells vis-á-vis the onset of pairing correlations in the neutron-excess nuclei. Whereas the 2p-2h

The HF as well as the perturbation theory results obtained with the [illegible] interactions for some nuclei in the 2p-1f and 2p-1f-1g shells.

Nucleus	E		$\langle Q_o^2 \rangle$		$\langle Q_o^2 \rangle_{max}$	(G_p, G_n)		ΔE		C^2_{2p-2h} (%)	
	V_{nn+pp}	V_{np}	V_{nn+pp}	V_{np}		V_{nn+pp}	V_{np}	V_{nn+pp}	V_{np}	V_{nn+pp}	V_{np}
					(a) Degenerate SPE's						
^{44}Ti	-04.64	-11.77	23.28	23.30	24.0	(1.5,1.5)	(3.7,3.7)	-0.58	-0.57	14.5	06.5
^{48}Ti	-11.03	-20.01	35.39	35.23	36.0	(1.4,1.5)	(1.9,0.7)	-0.88	-0.47	17.8	09.1
^{52}Fe	-17.40	-51.30	47.51	47.45	48.0	(1.5,1.5)	(4.0,4.0)	-1.17	-1.11	20.9	10.0
^{60}Zn	-02.42	-06.92	20.14	20.14	20.24	(1.1,1.1)	(2.1,2.1)	-0.50	-0.31	17.0	06.5
					(b) Experimental SPE's						
^{44}Ti	-1.54	-6.03	11.80	17.25	24.0	(0.4,0.4)	(1.8,1.8)	-1.56	-0.30	57.5	04.2
^{60}Zn	-1.05	-4.96	13.78	18.34	20.24	(0.3,0.3)	(1.8,1.8)	-0.68	-0.32	26.2	07.1
^{48}Ti	-3.83	-11.14	15.47	19.43	36.0	(0.4,0.4)	(0.9,0.5)	-1.64	-0.22	45.1	1.9

admixtures for ^{44}Ti resulting from the interaction V_{nn+pp} are only 14.5 percent with the degenerate SPE's, they increase to 57.5 percent when the experimental SPE's are used. The 2p-2h admixtures resulting from V_{nn+pp} for the nuclei ^{48}Ti and ^{60}Zn are also seen to increase significantly in going from a degenerate set of SPE's to the experimental one. In sharp contrast to these results, the 2p-2h admixtures due to V_{np} in fact decrease when we employ the experimental SPE's in place of the degenerate ones.

A number of Hartree-Fock-Bogoliubov calculations have been carried out in the recent past for the 2s-1d and 2p-1f shell nuclei. An important feature of these calculations is the treatment of pairing as well as the deformation effects on the same footing. These calculations have clearly established a link between the occurrence of non-rotational features and the extent of pairing correlations, as reflected in the HFB occupation probabilities and pairing gaps etc. in the N>Z nuclei in the 2s-1d and 2p-1f shells.

The results presented here, therefore, indicate that it is reasonable to attribute the observed departures from rotational behaviour in the neutron-excess nuclei in the A=16-60 mass region, to the significantly non-degenerate spectrum of the SPE's in this region.

II.7 Occurrence of Large Deformations in the Zirconium Region

The spherical SPE's in the Zr region are characterized by near-degeneracy; the spectrum of SPE's employed in a number

of successful shell-model studies in this region by Vergados and Kuo[17] as well as by Federman and Pittel[18] shows that five subshells, with a total occupancy of 32 like-particles, are clustered within just 4 MeV. In what follows we show that the emergence of the quasirotational spectra in this region can be understood, at least qualitatively, in terms of this feature of the SPE's.

We have verified that the interaction $V_{nn/pp} = -0.02\ b^{-4} q.q$, when employed in conjunction with the ^{41}Ca SPE's, can simulate the KB interaction reasonably well as far as the $\langle Q_0^2 \rangle$ values for various Ca isotopes are concerned. The intrinsic HF states resulting from this interaction (as well as those resulting from the KB interaction) are near-spherical. We have employed this interaction in a valence space spanned by the $1g_{9/2}$, $2d_{5/2}$, $3s_{1/2}$, $2d_{3/2}$, $1g_{7/2}$ and $1h_{11/2}$ orbits for neutrons. The nucleus ^{80}Zr has been considered to be an inert core. The SPE's employed are exactly the ones used in the earlier works[17,18], except for a slight lowering of the $1h_{11/2}$ energy by 0.4 MeV. The results of our HF calculations yield significantly small $\langle Q_0^2 \rangle$ values for the isotopes $^{90-98}Zr$; the quadrupole moments are always less than 18.7 b^2 whereas the maximum possible value for these isotopes ranges from about 47.6 b^2 to 62.7 b^2 for the given space. This is consistent with the observed near-spherical nature of these isotopes. For the nuclei $^{100,102}Zr$, however, we obtain significantly enhanced deformations; the computed $\langle Q_0^2 \rangle$ values are 53.3 and 64.7 percent of $\langle Q_0^2 \rangle_{max}$ respectively.

II.8 Conclusions

To summarize, we have shown that the like-particle interactions, often characterized as the "pairing" interactions, possess essentially the same deformation-producing tendency as the n-p interaction and that they both have a dominantly q.q character. Our calculations have revealed that the spectrum of spherical SPE's plays a very significant role vis-a-vis the relative importance of pairing correlations in the like-particle and the n-p channels. An appreciation of this role of the spherical SPE's is found instrumental in reconciling the near-spherical nature of the N>Z nuclei in the 2s-1d and 2p-1f shells with the onset of large deformations in highly neutron-rich Zr isotopes.

REFERENCES

1. P. Federman and S. Pittel, Phys. Lett. 69B, 385 (1977).
2. S.C.K. Nair, A. Ansari and L. Satpathy, Phys. Lett. 71B, 257 (1977).
3. S. Pittel, Nucl. Phys. A347, 417 (1980).
4. M. Danos and V. Gillet, Phys. Rev. 161, 1034 (1967).
5. A. Arima and V. Gillet, Ann. Phys. (NY) 66, 117 (1971).
6. A. Arima, T. Ohtsuka, F. Iachello and I. Talmi, Phys. Lett. 66B, 205 (1977).
7. E. Cheifetz, R.C. Jared, S.G. Thompson and J.B. Wilhelmy, Phys. Rev. Letters 25, 38 (1970).
8. S.K. Sharma and K.H. Bhatt, Phys. Lett. 36B, 550 (1971).
9. S.K. Sharma and K.H. Bhatt, Nucl. Phys. A192, 625 (1972).
10. A. Bohr and B. Mottelson, Kgl. Danske Videnskab. Selskab Mat. Phys. Medd. 27 (16) (1953) (3rd ed., 1964).
11. G. Ripka, in Advances in Nuclear Physics, edited by M. Baranger and E. Vogt (Plenum Press, New York-London, 1968), Vol. I.
12. T.T.S. Kuo, Nucl. Phys. A103, 71 (1967).
13. E.C. Halbert, J.B. McGrory, B.H. Wildenthal and S.P. Pandya, in Advances in Nuclear Physics, edited by M. Baranger and E. Vogt (Plenum Press, New York-London, 1971), Vol. IV.
14. M. Harvey, in Advances in Nuclear Physics, edited by M. Baranger and E. Vogt (Plenum Press, New York-London, 1968), Vol. 1, p.145.
15. T.T.S. Kuo and G.E. Brown, Nucl. Phys. A114, 241 (1968).

16. T.T.S. Kuo, private communication.

17. J.D. Vergados and Kuo, Phys. Lett. 35B, 93 (1971).

18. P. Federman and S. Pittel, Phys. Lett. 77B, 29 (1978).

CHAPTER III

MICROSCOPIC STUDY OF THE ONSET OF LARGE DEFORMATIONS IN THE ZIRCONIUM REGION

III.1 Introduction

In the last chapter we have mentioned that the significant degeneracy of the relevant spherical SPE's for A=80-100 nuclei offers the interesting possibility of building up sizable deformations in this region for even those nuclei which have only neutrons as valence particles. In this chapter we present explicit calculations of the yrast spectra in the isotopes of Zirconium and Molybdenum. This has been done with a view to achieve, at a quantitative level, a microscopic understanding of the fascinating shape-transition that appears to be occurring in this region.

In figure 1 we have given the observed low-lying spectra in some doubly-even isotopes of Zirconium and Molybdenum in the mass-range A=90-106. Whereas the spectra in A<96 have been known for quite some time now, the spectra for A≥98 nuclei were investigated relatively recently by Cheifetz et al.[1]

A striking feature of the spectra in $^{90-102}Zr$ is the sudden onset of deformation at N = 60; whereas one observes large energy separations (≥0.92 MeV) between the ground and the first excited states in $^{90-98}Zr$, the yrast spectra (with $J^{\pi}_{max} = 8^{+}$) in $^{100-102}Zr$ are almost rotational with

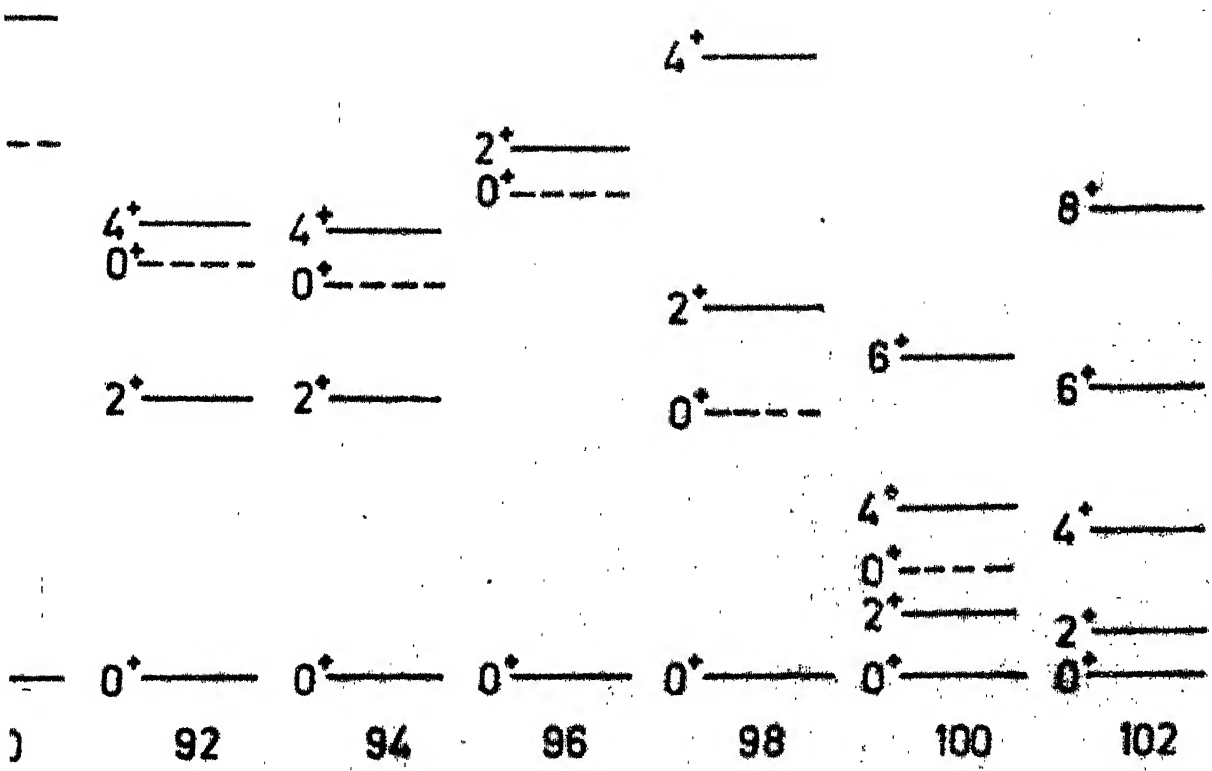

) Experimental spectra of the even Zr isotopes.

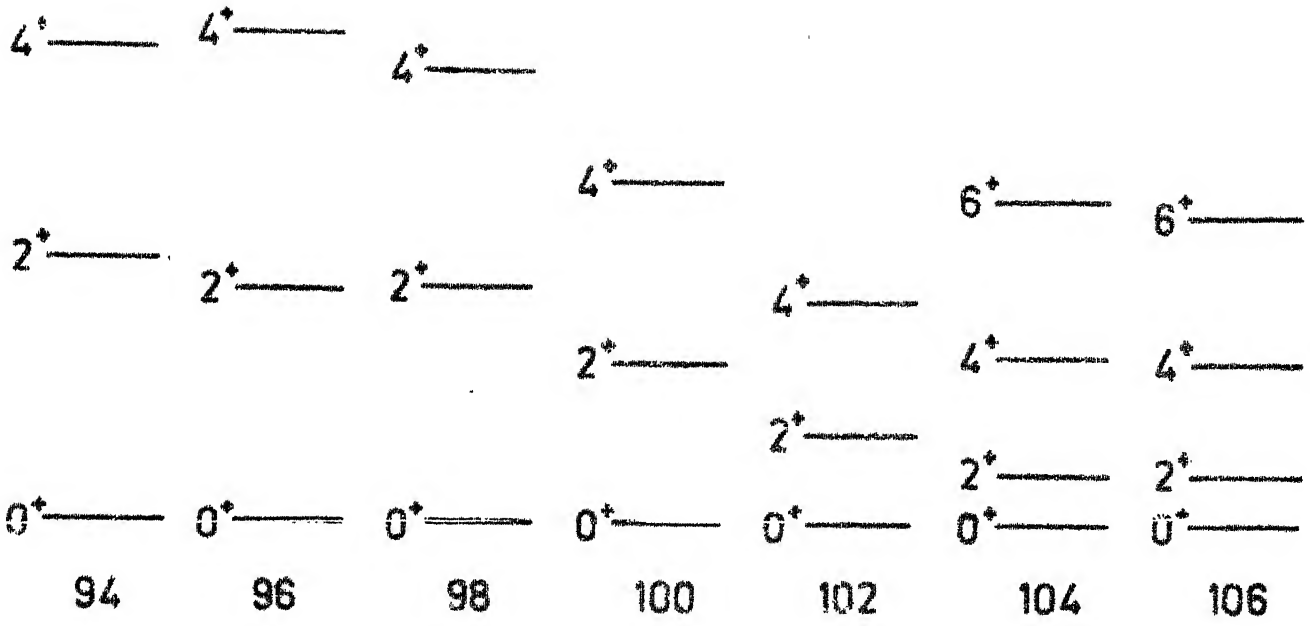

1(b) Experimental spectra of the even Mo isotopes.

$(E_{2+} - E_{0+}) = 0.21$ MeV. In the doubly-even Mo isotopes, on the other hand, one observes a distinct but gradual increase of deformation in going from A = 92 to A = 106.

The mass region A = 90-106 offers a nice example of shape transition. The region includes at the one end nuclei which are easily describable in terms of simple shell-model configurations.[2,3] At the other end of this region ($A \geq 100$) one comes across unambiguous evidence of rotational collectivity.

Microscopic calculations of the yrast spectra in the Zirconium region have not been attempted so far. However, some attempts have been made in the last few years with a view to identify some possible mechanisms that could be held responsible for the dramatic onset of large deformations at A = 100. In this connection, Federman and Pittel[4,7] have suggested that the onset of rotational features in the highly neutron-rich Zr isotopes may be crucially linked with the deformation of the Z = 40 proton core resulting from $\left[(1g_{9/2}) - (1g_{7/2})\right]_{T=0}$ interactions. Their calculation of the deformation energies[5] - and these were computed only for the Mo isotopes - also gave some indications regarding a possible connection between the onset of deformations at A = 102 and the T = 0 interactions in the $(1g_{9/2} - 1g_{7/2})$ and $(1g_{9/2} - 1h_{11/2})$ configurations .

The above calculation was performed assuming a ^{94}Sr inert core and employing as an effective interaction the

surface delta interaction. The active neutrons and protons were restricted to only the following orbits outside the ^{94}Sr core: $2p_{1/2}$, $1g_{9/2}$ and $2d_{5/2}$ for protons and $3s_{1/2}$, $2d_{3/2}$, $1g_{7/2}$ and $1h_{11/2}$ for neutrons.

Employing the above valence spaces for protons as well as neutrons, Federman, Pittel and Campos[6] have also carried out shell model calculations for the nucleus ^{98}Zr with a view to correlate the onset of deformation in $^{100,102}Zr$ with the increased involvement of $(1g_{9/2})^p$ $(1g_{7/2})^n$ configurations. In their shell model calculations the first-excited 0^+ level in ^{98}Zr (with E_x = 0.9 MeV) turns out to possess a wavefunction spread over many configurations. It is seen that the extent of configuration mixing in the 0_1^+ state depends very much on the relative single-particle energies of the $1g_{9/2}$ and $1g_{7/2}$ orbits. Having established a connection between the simultaneous occupation of the $(1g_{9/2})^p$ and $(1g_{7/2})^n$ orbits and the "collective" nature of the first-excited state in ^{98}Zr, Federman *et al.*[6] have conjectured that the rotational states in ^{100}Zr may also be possessing a structure quite similar to that of this state.

An important feature of the above calculations is the assumption that ^{94}Sr is a good core. The purpose of the present work is to examine the deformation systematics in the A = 90-106 mass region by employing a valence space large enough to permit an unbiased study of the shape transition. To this end we employ pairing-plus-quadrupole-quadrupole

interaction operative in a valence space spanned by the $2p_{1/2}$, $1g_{9/2}$, $2d_{5/2}$, $3s_{1/2}$, $2d_{3/2}$, $1g_{7/2}$ and $1h_{11/2}$ orbits for protons as well as neutrons. The nucleus ^{76}Sr has been considered to be an inert core.

The present calculation in the extended space is quite successful in reproducing the observed yrast spectra. A number of interesting features associated with the dramatic shape transitions in the Zirconium region are revealed. The results indicate unambiguously that the observed onset of large deformations in this region is not compatible with the assumption[4] of an inert ^{94}Sr core. Further, it turns out that, in contrast to the suggestions made by Federman and Pittel[5], the observed rotational spectra can be quite successfully explained without invoking strong T = 0 interactions for the $(1g_{9/2} - 1g_{7/2})$ configuration. The onset of deformation and the coexistence of deformed and spherical shapes in the A = 90-106 region are seen to be related mainly to the involvement of the $1h_{11/2}$ level, which possesses a large quadrupole content, in the valence space.

In section III.2 we discuss the choices of input parameters, such as the spherical SPE's and the pairing-plus-quadrupole-quadrupole effective interaction that we have employed in the present work. Section III.3 describes the Cranked Hartree-Fock (CHF) approximation which has been employed in carrying out some preliminary studies of deformation trends in the Zr isotopes. The CHF results in the space

$(3s\text{-}2d\text{-}1g\text{-}1h_{11/2})$ are discussed in section III.4. In section III.5 we discuss the Cranked Hartree-Fock-Bogoliubov (CHFB) prescription for studying the yrast spectra. In order to examine explicitly the role of protons vis-á-vis the onset of deformation in Zr isotopes, we have carried out CHFB calculations employing valence spaces that include also the $2p_{1/2}$ orbit in addition to the orbits included in the calculations discussed in section III.4. The results are presented in section III.6. Finally section III.7 contains some concluding remarks.

III.2 The Input Parameters of the Calculation

The spherical SPE's that we have used in our calculations are (in MeV): $\varepsilon(1g_{9/2}) = 0.0$, $\varepsilon(2d_{5/2}) = 5.4$, $\varepsilon(3s_{1/2}) = 6.4$, $\varepsilon(2d_{3/2}) = 7.9$, $\varepsilon(1g_{7/2}) = 8.4$ and $\varepsilon(1h_{11/2}) = 9.0$. This set of input SPE's is exactly the same as the one employed in a number of successful shell-model calculations by Vergados and Kuo[8] as well as by Federman and Pittel[5] except for a slight lowering of the $1h_{11/2}$ energy by 0.4 MeV.

The two-body effective interaction that we have employed is of "pairing + quadrupole-quadrupole" type. The quadrupole-quadrupole part of this schematic interaction has a tendency to give rise to the quadrupole deformations in nuclei and the pairing term favours sphericity since it acts only between a pair of nucleons in time-reversed orbits. The pairing part is given by

$$V_P = -\frac{1}{4} G \sum_{\alpha\beta} S_\alpha S_\beta C^+_\alpha C^+_{\bar{\alpha}} C_{\bar{\beta}} C_\beta \qquad \text{(III.2.1)}$$

Here 'α' stands for the set of quantum numbers (nljm). The state $\bar{\alpha}$ is the same as α but with the sign of m reversed: $\bar{\alpha}$ ≡ (nlj-m).

Further,

$$S_\alpha = (-1)^{j-m} \qquad \text{(III.2.2)}$$

The quadrupole-quadrupole part of the two-body interaction is given by

$$V_{q.q} = -\frac{1}{2}\chi \sum_{\alpha\beta\gamma\delta} \sum_{\mu=-2}^{+2} \langle\alpha|q^2_\mu|\gamma\rangle\langle\delta|q^2_{-\mu}|\beta\rangle(-1)^\mu c^+_\alpha c^+_\beta c_\delta c_\gamma \qquad \text{(III.2.3)}$$

The operator q^2_μ is given by

$$q^2_\mu = (16\pi/5)^{\frac{1}{2}} r^2 Y^2_\mu(\theta,\phi) \qquad \text{(III.2.4)}$$

The pairing-plus-quadrupole-quadrupole interaction leads to absurd consequences if it is allowed to operate in a complete set of states. Consider the pairing part of the interaction in the coordinate representation:

$$\langle \vec{r}'\uparrow,\ \vec{r}'\downarrow|V_p|\vec{r}\uparrow,\vec{r}\downarrow\rangle = -G \qquad \text{(III.2.5)}$$

The particles must be initially both at $\vec{r}$ and finally both at $\vec{r}'$ since they must be in time-reversed states. The constancy of the matrix element (III.2.5) - it has the value -G for arbitrarily large $|\vec{r}-\vec{r}'|$ - is clearly quite unphysical. The usage of this interaction is, however, justified for restricted spaces where it can simulate the effects due to the short-range components of the interaction. The quadrupole-quadrupole part also yields, via a Hartree type calculation, an effective quadrupole operator which is unbounded in a

complete set of oscillator states. Here again the interaction derives its validity from the limited size of the space. The optimum size of the oscillator space is usually two major shells[9]. Kumar and Baranger have shown that the matrix elements of the q.q force computed for two major shells are quite similar to the ones obtained from Hamada-Johnstone potential, using the G-matrix plus core polarization.

III.3 The Cranked Hartree-Fock (CHF) Method

In this section we present a brief outline of the CHF prescription that we have employed in the next section (subsection III.4.3) in order to examine some questions concerning the coexistence of the spherical and deformed states in $^{100,102}Zr$.

It was shown by Beck, Mang and Ring[10] and Villars and Schmeing-Rogerson[11] that the energy corresponding to a particular angular momentum (J) state projected from an intrinsic state ϕ which contains predominantly a K=0 ($K=\langle\phi|J_z|\phi\rangle$ = the projection of J along the body-fixed Z axes) state and small $K \neq 0$ components is approximately given by the following

$$E_J \equiv \frac{\langle\psi_J|H|\psi_J\rangle}{\langle\psi_J|\psi_J\rangle} \approx \langle\phi|H|\phi\rangle - \langle\phi|J_y^2|\phi\rangle/I$$

$$+ \omega'\left[\sqrt{J(J+1)} - \langle J_x\rangle\right] + \frac{1}{2I}\left[\sqrt{J(J+1)} - \langle J_x\rangle\right]^2 \qquad \text{(III.3.1)}$$

where

$$\omega' = \frac{\langle HJ_x\rangle - \langle H\rangle\langle J_x\rangle}{\langle J_y^2\rangle}, \quad \frac{1}{I} = \frac{\langle HJ_y^2\rangle - \langle H\rangle\langle J_y^2\rangle}{\langle J_y^2\rangle^2} \qquad \text{(III.3.2)}$$

Here the brackets < > imply that we are taking the expectation values with respect to the intrinsic state ϕ.

Now, carrying out HF type variations on E_J is equivalent to the cranked HF problem

$$\delta \left[<H - \omega J_x> \right] = 0 \qquad \text{(III.3.3)}$$

with the subsidiary condition

$$<J_x> = \sqrt{J(J+1)} \qquad \text{(III.3.4)}$$

provided the following two conditions are satisfied.

(i) The term $<J_y^2>/I$, which can be considered as a zero-point contribution to rotational energy, has no significant J dependence and hence can be treated as a constant during the variation on E_J ; and

(ii) The frequency ω appearing as the Lagrange multiplier in eq. (III.3.3), which is needed to satisfy the subsidiary condition (III.3.4), is the same as the ω' of eq. (III.3.1).

The condition (i) has been tested and found to be valid for some values of ω by Beck, Mang and Ring[10]. The condition (ii) has also been tested by Sharma *et al.*[12] in some 2s-1d and 2p-1f shell nuclei and found to be approximately valid.

In the present work we have solved the eq. (III.3.3) with the constraint (III.3.4) for some Zr isotopes by employing pairing-plus-quadrupole-quadrupole effective interactions in the 3s-2d-1g-$1h_{11/2}$ space.

III.4.1 A Preliminary Study of the Deformation Trends in the Doubly-even Zirconium and Molybdenum Isotopes

We discuss here first the results of our deformed HF calculations carried out by employing the pairing + q.q interaction. The strength χ (appearing in eq. (III.2.3) for like-particles was taken as $\chi_{nn} = -0.02$ MeV b^{-4} for the Zr isotopes. Here b is the oscillator parameter. The intrinsic states in Mo isotopes were computed by setting $\chi_{nn} = \chi_{pp} = -0.016$ MeV b^{-4} and $\chi_{np} = -0.0352$ MeV b^{-4}. In all these calculations the strength of the pairing interaction was fixed (through the approximate empirical relation $G = 18/A$) at $G = 0.18$ MeV.

The present calculations in the HF framework, in which the pairing effects have been ignored, are intended to serve only as a basis for a qualitative discussion of the deformation systematics in the Zirconium region. We shall see later, in section III.6, that the results are not drastically changed when we include the pairing effects.

We first discuss the nuclei ^{90,96}Zr. The observed spectra in these nuclei are characterized by large values ($\sim$2 MeV) of $(E_{2+} - E_{0+})$ separations. This can be interpreted in terms of sub-shell closures for the $1g_{9/2}$ and $2d_{5/2}$ orbits. The present calculation reproduces this feature - the minimum-energy HF solutions that we obtain for ^{90,96}Zr with the present set of input parameters are indeed spherical with the structures $(1g_{9/2})^{10}_{J=0}$ and $[(1g_{9/2})^{10}\ (2d_{5/2})^{6}]_{J=0}$ respectively.

The present approach differs significantly from that of earlier studies in that a light core (the nucleus ^{80}Zr) is assumed. However it is essential when using such a light core to first confirm that the calculations do reproduce the experimental "single-particle" spectra in the ^{90}Zr-plus-a nucleon system. In Table III.1 we have given the ^{91}Zr SPE's resulting from the relevant spherical HF solution. The calculated SPE's for various orbits compare favourably with the values obtained from the (d,p) as well as (p,p') reactions[13].

TABLE III.1

Comparison of the calculated ^{91}Zr SPE's with their experimental values

Neutron orbital	Energy (MeV)	
	Theory	Expt.
$2d_{5/2}$	0.00	0.00
$3s_{1/2}$	1.04	1.20
$2d_{3/2}$	2.30	2.08
$1g_{7/2}$	2.90	2.12

We next present the results for the nuclei $^{92,94,98-102}Zr$ and $^{92-106}Mo$ in Table III.2. Our calculation yields small $\langle Q_o^2 \rangle$ values for the nuclei $^{92,94,98}Zr$. This agrees with the observed lack of rotational collectivity in these nuclei. Note the sudden jump in the intrinsic $\langle Q_o^2 \rangle$ values in going from ^{98}Zr to ^{100}Zr; whereas the $\langle Q_o^2 \rangle$ value in ^{98}Zr is 18.74 b^2 out of a maximum value of 62.73 b^2 for the given space, that

TABLE III.2

The calculated values of the intrinsic quadrupole moments ($\langle Q_o^2 \rangle$) and the sub-shell occupation numbers for the Zr and Mo isotopes. Here $\langle Q_o^2 \rangle_{max}$ gives the maximum value of intrinsic quadrupole moment for each isotope. The quadrupole moments have been computed in units of b^2.

Isotope	$\langle Q_o^2 \rangle$	$\langle Q_o^2 \rangle_{max}$	Sub-shell occupancy			
			$1g_{9/2}$	$2d_{5/2}$	$1g_{7/2}$	$1h_{11/2}$
^{92}Zr	14.5	51.7	9.94	1.49	0.01	0.0
^{94}Zr	17.0	55.6	9.96	3.25	0.06	0.0
^{98}Zr	18.8	62.7	9.99	5.53	0.65	0.0
^{100}Zr	32.0	62.6	9.76	3.89	1.82	2.0
^{102}Zr	38.9	60.6	9.65	3.59	2.62	4.0
^{92}Mo	12.7	63.6	9.84	0.14	0.0	0.0
^{94}Mo	31.9	67.6	9.66	1.13	0.14	0.0
^{96}Mo	41.4	71.6	9.61	1.66	1.24	0.0
^{98}Mo	45.7	75.6	9.78	2.57	1.60	0.0
^{100}Mo	53.6	78.7	9.73	2.41	1.76	2.0
^{102}Mo	59.8	78.6	9.68	2.31	1.87	4.0
^{104}Mo	59.5	76.6	9.76	3.27	2.82	4.0
^{106}Mo	62.9	74.6	9.74	3.26	2.84	6.0

for the nucleus ^{100}Zr is 31.97 b^2 which is roughly 50 percent of the $\langle Q_o^2 \rangle_{max}$ in this nucleus. The present results, therefore, explain, at least qualitatively, the experimentally observed dramatic onset of large deformations at ^{100}Zr.

The results for the nuclei $^{92-106}Mo$ also reproduce successfully the deformation trends that are implied by the observed spectra. The nuclei $^{102-106}Mo$ display well-developed rotational spectra. This is easily explained qualitatively in the present calculation where we obtain large intrinsic deformations - roughly 80 percent of the maximum possible values - for these nuclei.

The reason for the sudden increase in intrinsic deformations at N = 60 now becomes immediately obvious if one considers the subshell occupancies for the $1h_{11/2}$ orbit given in column 7, Table III.2. The nuclei ^{100}Zr and ^{102}Zr have two and four neutrons in the orbit $1h_{11/2}$ respectively. Whereas the sudden change in the $1h_{11/2}$ occupancy in going from ^{98}Zr to ^{100}Zr is seen to lead to an increase of about 65 percent in the computed $\langle Q^2 \rangle$ values, a further change of the occupancy in going from ^{100}Zr to ^{102}Zr results in an increase of about 20 percent. The effective Nilsson deformations for the nuclei $^{100,102}Zr$ consistent with the computed $1h_{11/2}$ occupancies are shown in figure 2.

The results for the $1h_{11/2}$ sub-shell occupancies in the Mo isotopes further emphasize the role of the $1h_{11/2}$ orbit in producing large deformations - and the associated

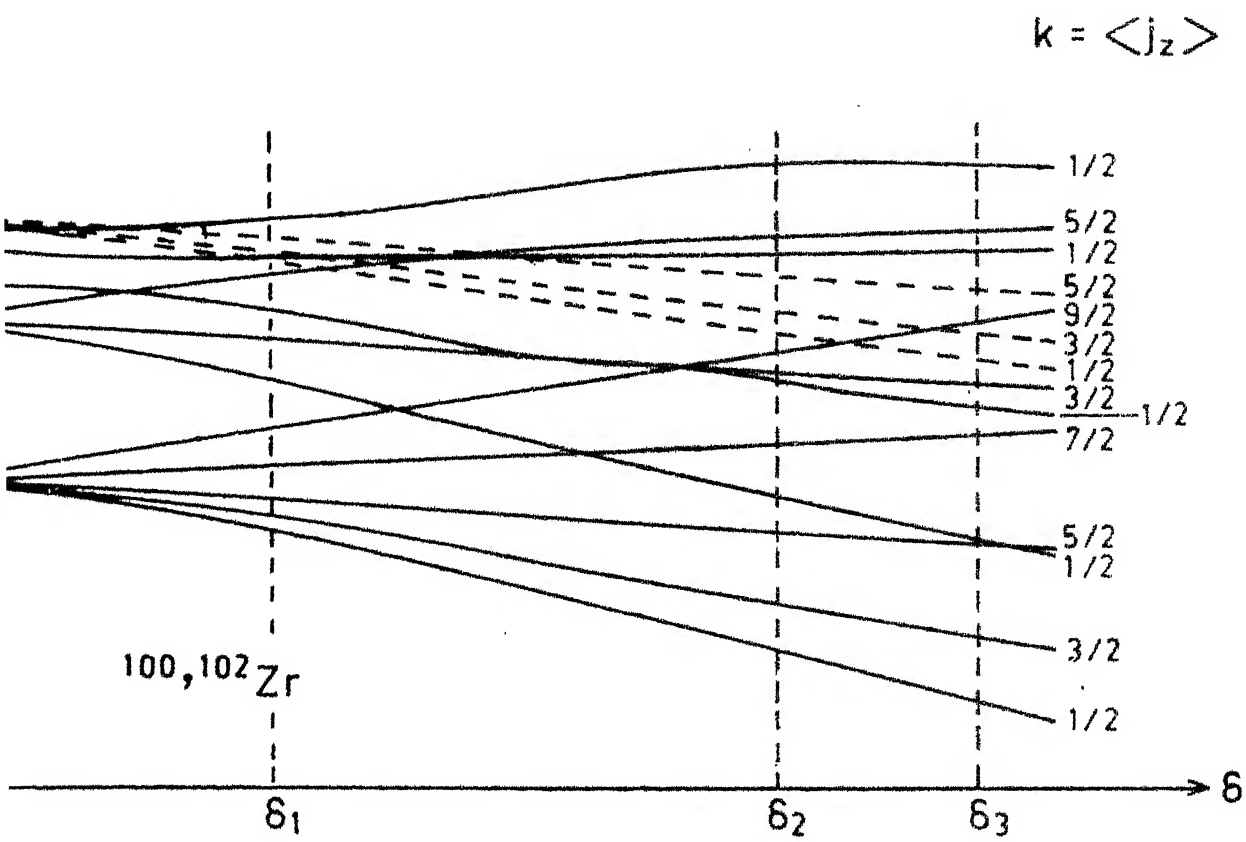

Comparison of the deformations of the HF states of the N=60 and 62 isotopes of Zr. The values of $k = \langle j_z \rangle$ are given on the right..

quasirotational features - in the A = 90-106 region. In view of the fact that ^{106}Mo already has six neutrons in the $1h_{11/2}$ orbit, one expects a decrease in the $\langle Q_o^2 \rangle$ values in the heavier Mo isotopes.

The calculated results for the sub-shell occupancies for the $1g_{9/2}$, $2d_{5/2}$ and $1g_{7/2}$ orbits in the Zr and Mo isotopes (see columns 4-6, Table III.2) indicate that the nucleus ^{90}Zr can approximately be considered an inert core even in the quasirotational isotopes $^{100-102}$Zr and $^{102-106}$Mo; the maximum depletion of the $1g_{9/2}$ orbit is seen to be only about 3 percent in these isotopes. The $2d_{5/2}$ occupancies in $^{98-106}$Mo are, however, seen to range only between 2.57 and 3.26. This shows that the usual assumption[4-6] of an inert ^{94}Sr core is not valid for nuclei with N≥56.

III.4.2 The Role of T=0 Interactions in Producing Deformations in Molybdenum Isotopes

In the earlier work[5,7] in which the surface delta interaction was employed in conjunction with ^{94}Sr core, the T = 0 interaction had turned out to be the major source of deformations in the Mo isotopes. In order to assess the role of this component of the interaction in producing deformations in the context of present calculation which involves an extended space, we have obtained the HF states for $^{100-106}$Mo with the full interaction as well as the T = 0 part alone. The results are given in Table III.3.

TABLE III.3

The $\langle Q_o^2 \rangle$ values in some Mo isotopes calculated with the full interaction (V_{full}) as well as its T = 0 component ($V_{T=0}$)

	^{100}Mo	^{102}Mo	^{104}Mo	^{106}Mo
V_{full}	53.59	59.79	59.49	62.86
$V_{T=0}$	09.78	18.59	22.58	21.00

We find that the T = 0 part plays only a minor role in producing deformations in the Mo isotopes. This relative suppression in the deformation producing role of the T = 0 component in the present case is closely related to the fact that the choice of ^{80}Zr as a core leads to a reduction in the numbers of n-p pairs in comparison to the n-n and p-p ones.

III.4.3 The First-excited 0^+ Levels in the Doubly-even Isotopes of Zirconium

A significant feature which characterizes the experimental spectra in the nuclei $^{90-100}$Zr is the occurrence of an excited 0^+ level at rather low energies. In ^{96}Zr the first 0^+ level occurs at 1.59 MeV, at roughly the same energy as in the nuclei $^{90-94}$Zr. In ^{98}Zr, however, this level appears at 0.85 MeV and in ^{100}Zr it suddenly drops to just 0.33 MeV.

Federman, Pittel and Campos[6] have recently tried to examine the nature of the first-excited 0^+ level in the nucleus ^{98}Zr in the framework of shell-model by considering

the nucleus ^{94}Sr to be an inert core. Their calculation indicates a "collective" nature for this state in the sense that it is made up of a large number of shell-model configurations. However no calculations have so far been carried out to study, in a systematic manner, the $(E_{0^+} - E_{0^+})$ trends for the nuclei $^{92-98}Zr$.

We present here an HF-oriented study of the excitation energies of the first 0^+ levels. In Table III.4 we give the results concerning the position of the first excited 0^+ levels in the nuclei $^{92-102}Zr$. The 0^+ positions in the nonrotational nuclei $^{92-98}Zr$ have been obtained by computing the difference in energies between the minimum-energy HF state and the lowest 1 particle- 1 hole state with $K = 0$. The excited 0^+ levels in the quasirotational nuclei $^{100,102}Zr$ have been calculated by obtaining the non-axial, excited HF solutions. It may be mentioned here that an explicit inclusion of the pairing correlations is not likely to affect our estimates for the $(0^{+'}-0^+)$ separation. This is because the pairing correlations are expected to lead to a lowering of the two HF intrinsic minima (or a HF state and a 1p-1h state) by approximately equal amounts.

TABLE III.4

Comparison of the calculated as well as the observed positions (in MeV) of the first excited 0^+ states in the Zirconium isotopes

	^{92}Zr	^{94}Zr	^{96}Zr	^{98}Zr	^{100}Zr	^{102}Zr
Calculated	2.27	2.22	2.14	1.66	0.53	1.62
Experimental	1.40	1.32	1.62	0.86	0.33	>1.50

The results concerning the $0^{+'}$ positions are in good qualitative agreement with the experiments - the sudden drop in the excited 0^+ position in ^{98}Zr, after remaining virtually constant in $^{92-96}Zr$, is reproduced. In ^{100}Zr the excited 0^+ lies at 0.53 MeV in the calculated spectrum, in reasonable agreement with the experiments. This 0^+ state is seen to arise from a weakly-deformed intrinsic state (with $\langle Q_o^2 \rangle = 16.8\ b^2$). In view of the highly deformed nature of the ground state band in ^{100}Zr, this nucleus appears to provide an example of the coexistance of the shapes with widely varying degrees of deformation. As discussed earlier, the addition of two more $1h_{11/2}$ neutrons to ^{100}Zr leads to a significant increase in the intrinsic deformation of the yrast levels. This leads to a further lowering of the yrast 0^+ state relative to the excited one since the latter has a nearly-spherical parentage. Thus the excited 0^+ lies at 1.62 MeV in the calculated spectrum. Importantly enough, no excited 0^+ has so far been reported in ^{102}Zr at least upto 1.55 MeV of excitation.

In figure 3 we display the theoretical yrast spectra that we have computed for the deformed nuclei $^{100,102}Zr$ in the framework of the CHF procedure discussed in section III.3. Various non-axial intrinsic states, $\phi(\omega)$, were obtained by solving the equation III.3.3 — and this is just the HF equation for the Hamiltonian $(H-\omega J_x)$ — for various values of ω. The intrinsic states for various yrast levels were then obtained by subjecting various $\phi(\omega)$'s to the constraint III.3.4.

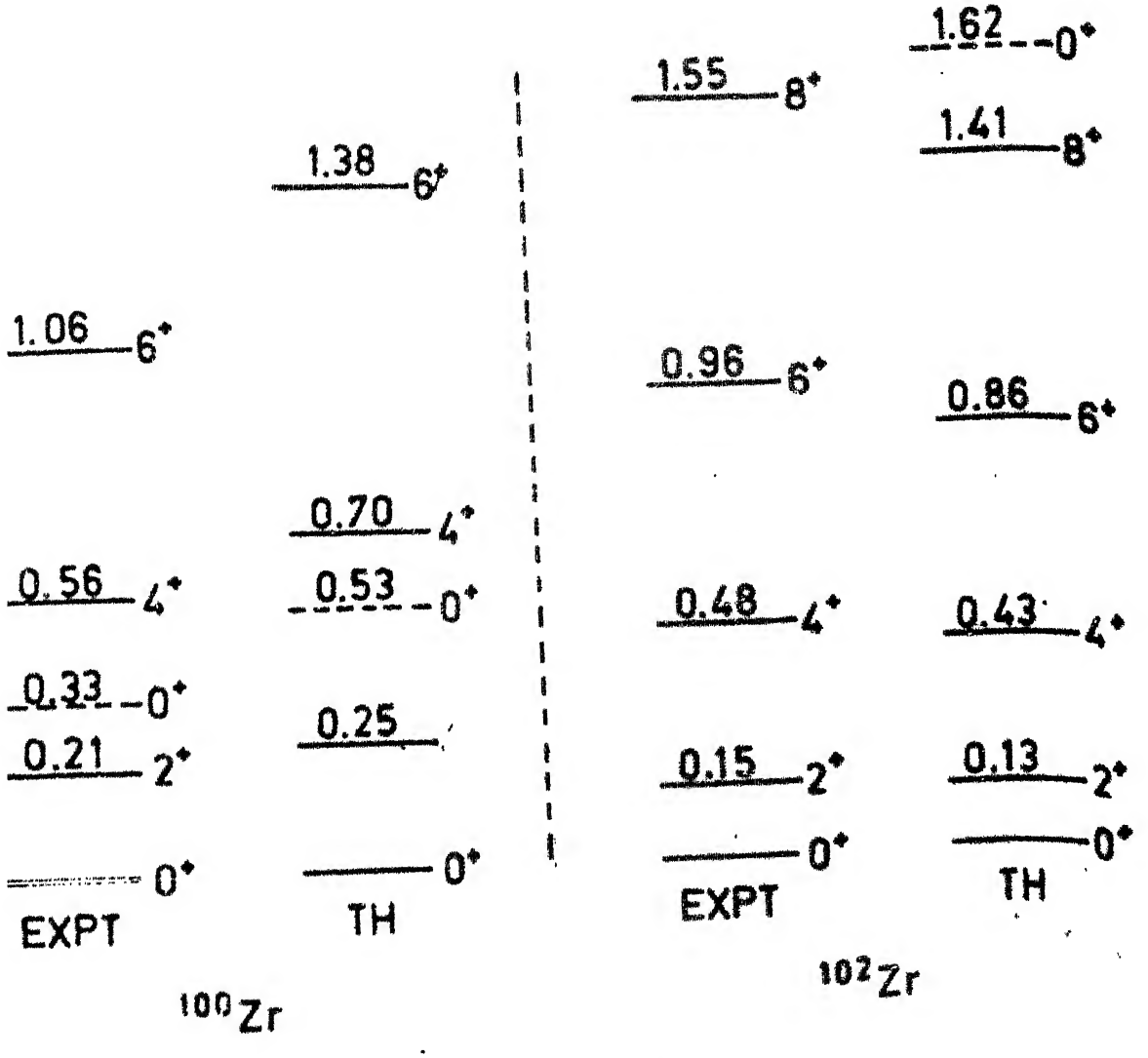

Comparison of the calculated and the experimental yrast spectra in nuclei ^{100}Zr and ^{102}Zr.

The results for the nuclei $^{100,102}Zr$ are presented in Table III.5.

It is interesting to see that the present CHF calculation, which is rather elementary in the sense that it ignores pairing effects as well as the participation of the Z=40 core protons, leads to the computed spectra which are in reasonable agreement with the experiments. The calculation reproduces the observed positions of all the yrast levels, except the $J^{\pi}=6^{+}$ level in ^{100}Zr, within an accuracy of 140 keV.

III.5.1 The Cranked Hartree-Fock-Bogoliubov (CHFB) Method

In this section we discuss the general CHFB theory which is applicable for any given two-body effective interaction[14].

Consider the many-body Hamiltonian

$$H = \Sigma_i \langle i|\epsilon|i\rangle a_i^+ a_i + \frac{1}{4} \Sigma_{ijkl} \langle ij|V_a|kl\rangle a_i^+ a_j^+ a_l a_k \quad \text{(III.5.1)}$$

The indices "ijkl" span the active valence single-particle states contained in the model space, and a_i^+ and a_i are the particle creation and annihilation operators respectively. The effective nucleon-nucleon interaction V appropriate for the model space is antisymmetrized, so that

$$\langle ij|V_a|kl\rangle = \langle ij|V|kl\rangle - \langle ij|V|lk\rangle \quad \text{(III.5.2)}$$

The main idea involved in the CHFB or HFB theory is to obtain a transformation from particle co-ordinates to quasiparticle co-ordinates such that the quasiparticles are

relatively weakly interacting. That is we want to express H as

$$H = E_o + H_{qp} + H_{qp\text{-}int} \qquad \text{(III.5.3)}$$

where E_o is the energy of the quasiparticle vacuum, H_{qp} describes the elementary quasiparticle excitations, and $H_{qp\text{-}int}$ characterizes what we hope is a weak interaction between quasiparticles. In HFB this last term is neglected, so that H is approximated by an independent quasiparticle Hamiltonian. It is obvious that the neglect of $H_{qp\text{-}int}$ will result in a loss of symmetry - the Hamiltonian $(H_o + H_{qp})$ will not possess, in general, the same symmetries as the initial Hamiltonian H.

Just as in the BCS theory, HFB includes pairing correlations by introducing number nonconserving wave functions. The Hamiltonian H is replaced by

$$H' = H - \lambda_p N_p - \lambda_n N_n \qquad \text{(III.5.4)}$$

where the Lagrange multipliers λ_p and λ_n turn out to have the physical interpretation of proton and neutron Fermi energies. The Lagrange multipliers are adjusted so that the number operators

$$N_p = \sum_i a^+_{ip} a_{ip} \,, \quad N_n = \sum_i a^+_{in} a_{in} \qquad \text{(III.5.5)}$$

have the expectation values

$$\langle \Phi_o | N_p | \Phi_o \rangle = Z \,, \quad \langle \Phi_o | N_n | \Phi_o \rangle = A\text{-}Z \qquad \text{(III.5.6)}$$

where $|\Phi_o\rangle$ is the quasiparticle vacuum.

The independent quasiparticle Hamiltonian is, in general, not rotationally invariant. Therefore angular momentum is not a good quantum number for $|\Phi_o\rangle$. The Inglis cranking model[15-16] is invoked to approximate angular momentum projection. Define

$$H' = H - \lambda_p N_p - \lambda_n N_n - \omega J_x \qquad \text{(III.5.7)}$$

where the Lagrange multiplier ω is adjusted so that the angular momentum component

$$\hat{J}_x = \sum_{ij} \langle i|J_x|j\rangle a_i^+ a_j \qquad \text{(III.5.8)}$$

has the expectation value

$$\langle\Phi_o|J_x|\Phi_o\rangle = \sqrt{J(J+1)} \qquad \text{(III.5.9)}$$

The expressions given above correspond to the intuitive picture of a nucleus that rotates with angular velocity ω about the x axis. Mang[17] has shown that the cranking prescription also results when one considers an appropriate approximate treatment of angular momentum projection.

Although the mean value of angular momentum in the y and z directions vanishes,

$$\langle\Phi_o|J_y|\Phi_o\rangle = \langle\Phi_o|J_z|\Phi_o\rangle = 0, \qquad \text{(III.5.10)}$$

there may be significant angular momentum fluctuations in these directions. The cranking term $(-\omega J_x)$ violates time reversal, which technically complicates the calculation of the HFB intrinsic state.

III.5.2 Derivation of the CHFB equations

We next demonstrate how the schematic separation of the Hamiltonian, indicated in equation (III.5.3), can be realized. A quasiparticle is an excitation of the system. In the vacuum state appropriate to HF theory, all single-particle levels $|\alpha>$ below the Fermi energy ε_F are occupied, and all levels above ε_F are empty. Thus in the HF theory the quasiparticle creation operators q_α^+ are defined by

$$q_\alpha^+ = \begin{cases} a_\alpha^+ & (\varepsilon_\alpha > \varepsilon_F) \qquad \text{(III.5.11a)} \\ a_\alpha & (\varepsilon_\alpha < \varepsilon_F) \qquad \text{(III.5.11b)} \end{cases}$$

where (III.5.11a) signifies creation of a particle and (III.5.11b) represents creation of a hole.

In BCS theory the quasiparticles are defined by the special Bogoliubov transformation

$$q_\alpha^+ = U_\alpha\, a_\alpha^+ - V_\alpha\, a_{\bar{\alpha}} \qquad \text{(III.5.12)}$$

where $|\bar{\alpha}>$ is the time reverse of $|\alpha>$, and U_α and V_α are real.

The HFB theory employs the general Bogoliubov transformation

$$q_i^+ = \sum_j (U_{ij}\, a_j^+ + V_{ij}\, a_j) \qquad \text{(III.5.13)}$$

in which each quasiparticle is a linear combination of all particle creation and destruction operators. If there are N single-particle basis states, then U and V are N x N complex matrices, and $\hat{q}$ and $\hat{a}$ are N-component vectors.

The 2N x 2N linear transformation

$$\begin{Bmatrix} q^+ \\ q \end{Bmatrix} = \begin{bmatrix} U & V \\ V^* & U^* \end{bmatrix} \begin{Bmatrix} a^+ \\ a \end{Bmatrix} \quad . \qquad \text{(III.5.14)}$$

is required to be unitary. Equations (III.5.14) can then be inverted to express the particle operators in terms of the quasiparticle operators

$$a_i^+ = \sum_j (U^*_{ji} \, q_j^+ + V_{ji} \, q_j) \qquad \text{(III.5.15)}$$

The unitarity constraints are

$$UU^+ + VV^+ = U^+U + \tilde{V}V^* = I \qquad \text{(III.5.16)}$$

$$U\tilde{V} + V\tilde{U} = U^+V + \tilde{V}U^* = 0 \qquad \text{(III.5.17)}$$

where U^* denotes complex conjugate and $\tilde{U}$ denotes the transpose of U. These equations may also be derived by requiring the particle and quasiparticle operators to satisfy the fermion anticommutation relations

$$[a_i^+ , a_j] = \delta_{ij} , [a_i^+, a_j^+] = [a_i, a_j] = 0 \qquad \text{(III.5.17)}$$

$$[q_i^+ , q_j] = \delta_{ij} , [q_i^+, q_j^+] = [q_i , q_j] = 0 \qquad \text{(III.5.18)}$$

The quasiparticle vacuum $|\Phi_o\rangle$ is defined by the requirement

$$q_i |\Phi_o\rangle = 0 \quad \text{(for all i)} \qquad \text{(III.5.19)}$$

From eq. (III.5.18) it follows that the solution of eq. (III.5.19) is

$$|\Phi_o\rangle = N \prod_i q_i |0\rangle \qquad \text{(III.5.20)}$$

where N is a normalization constant and $|0\rangle$ is the particle vacuum.

The density matrix ρ and the pairing tensor t are defined by

$$\rho_{ij} = \langle \Phi_o | a_j^+ a_i | \Phi_o \rangle \qquad \text{(III.5.21)}$$

$$t_{ij} = \langle \Phi_o | a_j a_i | \Phi_o \rangle \qquad \text{(III.5.22)}$$

It follows that ρ is hermitian and t is antisymmetric. Also t is nonzero only for number nonconserving wave functions. To evaluate ρ and t, substitute eq. (III.5.15) into eqs. (III.5.21), (III.5.22) and apply eqs. (III.5.17), (III.5.18).

The result is

$$\rho = V^+ V \qquad \text{(III.5.23)}$$

$$t = V^+ U \qquad \text{(III.5.24)}$$

The constrained Hamiltonian is defined by

$$H' = H - C \qquad \text{(III.5.25)}$$

$$C = \lambda_p N_p + \lambda_n N_n + \omega J_x \qquad \text{(III.5.26)}$$

where H is given by eq. (III.5.1). By substituting eqs. (III.5.21), (III.5.22) into eq. (III.5.25), H' can be expressed as

$$H' = H'_o + H'_2 + H'_4 \qquad \text{(III.5.27)}$$

where H'_n contains n uncontracted operators, and

$$H'_o = \mathrm{Tr}\left[\left(\varepsilon - C + \frac{\Gamma}{2}\right)\rho + \frac{1}{2}\Delta t^+\right] \qquad \text{(III.5.28)}$$

$$H'_2 = \sum_{ij} (X - C)_{ij} :a_i^+ a_j: + \frac{1}{2} \sum_{ij} \Delta_{ij} :a_i^+ a_j^+: + \frac{1}{2} \sum_{ij} \Delta_{ij}^+ :a_i a_j: \qquad \text{(III.5.29)}$$

$$H_4' = \frac{1}{4} \sum_{ijkl} \langle ij|V_A|kl\rangle : a_i^+ a_j^+ a_l a_k : \qquad \text{(III.5.30)}$$

The HF Hamiltonian X, the HF potential Γ and the pair potential Δ are defined by

$$X = \varepsilon + \Gamma \qquad \text{(III.5.31)}$$

$$\Gamma_{ij} = \sum_{kl} \langle ik|V_a|jl\rangle \rho_{lk} \qquad \text{(III.5.32)}$$

$$\Delta_{ij} = \frac{1}{2} \sum_{kl} \langle ij|V_a|kl\rangle t_{kl} \qquad \text{(III.5.33)}$$

It follows that X and Γ are hermitian and that Δ is antisymmetric. For any normal product :O:, the expectation value $\langle \Phi_o| :O: |\Phi_o\rangle$ vanishes by construction. Consequently $\langle \Phi_o| H_2' + H_4' |\Phi_o\rangle = 0$, so that the vacuum expectation value $\langle \Phi_o|H'|\Phi_o\rangle$ is H_o'. The quasiparticle vacuum energy is

$$\langle \Phi_o|H|\Phi_o\rangle = \langle \Phi_o|H' + C|\Phi_o\rangle = \mathrm{Tr}[(\varepsilon + \tfrac{1}{2}\Gamma)\rho + \tfrac{1}{2}\Delta t^+] \qquad \text{(III.5.34)}$$

The first term on the right-hand side is the HF binding energy, and the second term is the pairing energy.

The quasiparticle excitation energies are obtained from H_2'. The remainder H_4' describes the quasiparticle interactions, which are neglected in HFB.

As mentioned earlier our aim here is to express H' as

$$H' = H_o' + \sum_i E_i q_i^+ q_i + H_{qp\text{-}int.} \qquad \text{(III.5.35)}$$

This will be achieved if H_2' acquires the form of an independent quasiparticle Hamiltonian

$$H_2' = \sum_i E_i q_i^+ q_i \qquad \text{(III.5.36)}$$

Inserting eq. (III.5.36) into the commutator $\left[H_2', q_i^+\right]$, we have

$$\left[H_2', q_i^+\right] = E_i q_i^+ = E_i \sum_j (U_{ij} a_j^+ + V_{ij} a_j) \quad \text{(III.5.37)}$$

Alternatively, using eq. (III.5.29) we obtain

$$\left[H_2', q_i^+\right] = \sum_{jk} \left[(X - C)_{jk} U_{ik} + \Lambda_{jk} V_{ik}\right] a_j^+ + \sum_{jk} \left[-\Delta_{jk}^* U_{ik} - (X - C)_{jk}^* V_{ik}\right] a_j \quad \text{(III.5.38)}$$

Equating the coefficients of a_j^+ and a_j in eqs. (III.5.37) and (III.5.38) we have

$$\begin{bmatrix} X - C & \Lambda \\ -\Lambda^* & -(X - C)^* \end{bmatrix} \begin{bmatrix} \vec{U}_i \\ \vec{V}_i \end{bmatrix} = E_i \begin{bmatrix} \vec{U}_i \\ \vec{V}_i \end{bmatrix} \quad \text{(III.5.39)}$$

where $\vec{U}_i$ denotes the vector $(U_{i1}, U_{i2} \cdots U_{iN})$ and N is the number of single-particle states and similarly for $\vec{V}_i$. These are the HFB equations.

We now discuss several simplifications which result provided one exploits certain symmetries associated with the J_x operator. We also make use of the simplified nature of the interaction.

III.5.3 Symmetries

It is convenient to separate the harmonic oscillator states into two sets. The first set contains the states $|k>$, which are now restricted to have $(m - \frac{1}{2})$ equal to an even integer. The second set contains the time-reversed states $|\bar{k}> = T|k>$, which have $(m - \frac{1}{2})$ equal to an odd integer.

The phase convention is $T|nljm_\tau\rangle = (-1)^{j-m+1}|nlj-m_\tau\rangle$. For quasiparticle operators of the form

$$q_i^+ = \sum_k (U_{ik}\, a_k^+ + V_{ik}\, a_{\bar{k}}) \qquad \text{(III.5.40)}$$

$$q_{\bar{i}}^+ = \sum_k (\bar{U}_{ik}\, a_{\bar{k}}^+ + \bar{V}_{ik}\, a_k) \qquad \text{(III.5.41)}$$

ρ does not connect the set of states $|k\rangle$ and $|\bar{k}\rangle$. For t, however, only the matrix elements connecting $|k\rangle$ and $|\bar{k}\rangle$ are non-zero. Since the nucleon-nucleon interaction conserves angular momentum, the average potentials (Γ,Δ) follow the partitioning of the densities (ρ,t). That is

$$\rho = \begin{pmatrix} \rho_1 & 0 \\ 0 & \rho_2 \end{pmatrix}, \quad t = \begin{pmatrix} 0 & t_1 \\ t_2 & 0 \end{pmatrix}$$

$$X = \begin{pmatrix} X_1 & 0 \\ 0 & X_2 \end{pmatrix}, \quad \Delta = \begin{pmatrix} 0 & \Delta_1 \\ \Delta_2 & 0 \end{pmatrix} \qquad \text{(III.5.42)}$$

where ρ and X are hermitian. Substituting (III.5.42) into the HFB equations demonstrates that the energy matrix decomposes into two blocks and that the eigen-vectors retain the form of eqs (III.5.40), (III.5.41). Consequently the partitioning propagates through each iteration.

Time reversal symmetry is imposed by requiring that

$$q_{\bar{i}}^+ = T\, q_i^+\, T^{-1} \qquad \text{(III.5.43)}$$

so that

$$\bar{U}_{ik} = U_{ik}^* \; ; \; \bar{V}_{ik} = -V_{ik}^* \qquad \text{(III.5.44)}$$

Then the quasiparticle vacuum is time-reversal invariant, and

$$\rho_2 = \rho_1^* \, , \; X_2 = X_1^* \, , \; t_1^+ = t_1 \, , \; \Delta_1^+ = \Delta_1 \qquad \text{(III.5.45)}$$

Consequently only the block of the energy matrix corresponding to eq. (III.5.40) need be diagonalized

$$\begin{bmatrix} X_1 - C & \Delta_1 \\ \Delta_1 & -(X_1 - C) \end{bmatrix} \begin{bmatrix} \vec{U}_i \\ \vec{V}_i \end{bmatrix} = E_i \begin{bmatrix} \vec{U}_i \\ \vec{V}_i \end{bmatrix} \qquad \text{(III.5.46)}$$

From eqs (III.5.45) it follows that the time reversed quasiparticles q_i^+ and $q_{\bar{i}}^+$ are degenerate

$$E_{\bar{i}} = E_i \qquad \text{(III.5.47)}$$

By using eq. (III.5.45) along with the unitarity constraints on t_1 and ρ_1 , we find that ρ_1 and t_1 commute. So a basis $|\alpha\bar{\alpha}>$ exists, where

$$a_\alpha^+ = \sum_k D_{\alpha k} \, a_k^+ \qquad \text{(III.5.48)}$$

$$a_{\bar{\alpha}}^+ = \sum_k D_{\alpha k}^* \, a_{\bar{k}}^+ \qquad \text{(III.5.47)}$$

such that ρ and t have the canonical form. The constraint $\rho - \rho^2 = tt^+$ implies that

$$|t_{\alpha\bar{\alpha}}| = [\rho_\alpha (1 - \rho_\alpha)]^{\frac{1}{2}} \qquad \text{(III.5.50)}$$

which further indicates that the HFB quasiparticle vacuum may be expressed in the BCS form

$$|\phi_o> = \prod_\alpha (U_\alpha + V_\alpha \, a_\alpha^+ \, a_{\bar{\alpha}}^+)|0> \qquad \text{(III.5.51)}$$

The paired orbitals are now related by time reversal.

A wave function is defined to have triaxial symmetry if it is invariant, except for a multiplicative phase factor, with respect to rotation by π about each of the three principal axes $R_i(\pi)$ and reflection through each of the three principal planes σ_i, where

$$R_i(\pi) = \exp(-i\pi J_i) \qquad \text{(III.5.52)}$$

$$\sigma_i = P\, R_i(\pi) \qquad \text{(III.5.53)}$$

Here i denotes x,y,z and σ_x is reflection through the yz-plane.

The effect of $R_i(\pi)$ on the single-particle state $|jm\rangle$ is given by

$$R_x(\pi)\,|jm\rangle = e^{-i\pi j}\,|j-m\rangle \qquad \text{(III.5.54)}$$

$$R_y(\pi)\,|jm\rangle = (-1)^{j-m}\,|j-m\rangle \qquad \text{(III-5.55)}$$

$$R_z(\pi)\,|jm\rangle = e^{-i\pi m}\,|jm\rangle \qquad \text{(III.5.56)}$$

Since $|k\rangle$ is restricted to states with $(m - \frac{1}{2})$ even, the particle operators transform under $R_z(\pi)$ as

$$R_z(\pi) \begin{Bmatrix} a_k^+ \\ a_{\bar{k}} \end{Bmatrix} R_z^{-1}(\pi) = -i \begin{Bmatrix} a_k^+ \\ a_{\bar{k}} \end{Bmatrix} \qquad \text{(III.5.57a)}$$

$$R_z(\pi) \begin{Bmatrix} a_{\bar{k}}^+ \\ a_k \end{Bmatrix} R_z^{-1}(\pi) = +i \begin{Bmatrix} a_{\bar{k}}^+ \\ a_k \end{Bmatrix} \qquad \text{(III.5.57b)}$$

Consequently the quasiparticle operators q_i^+ and $q_{\bar{i}}^+$ are invariant with respect to $R_z(\pi)$ and therefore so is the vacuum $|\phi_o\rangle$. Also notice that $\sigma_y\,|jm\rangle = T\,|jm\rangle$, so that σ_y and T are equivalent if the quasiparticle coefficients U and V are chosen to be real.

To summarize, if the quasiparticle operators are chosen as

$$q_i^+ = \sum_k (U_{ik}\, a_k^+ + V_{ik}\, a_{\bar{k}}) \qquad \text{(III.5.58)}$$

$$q_{\bar{i}}^+ = \sum_k (U_{ik}\, a_{\bar{k}}^+ - V_{ik}\, a_k) \qquad \text{(III.5.59)}$$

where U and V are real and $(m_k - \frac{1}{2})$ is even, and if each quasiparticle operator contains particle operators possessing the same parity, then the HFB vacuum $|\phi_o\rangle$ is time-reversal invariant and triaxially symmetric.

The self-consistent symmetries discussed above are the ones satisfied by H. The constrained Hamiltonian H' (eq. III.5.4) violates most of the symmetries mentioned here. For instance J_x anticommutes with the following operators: time reversal, rotations about y and z axes and reflection through the xy and xz planes. Therefore cranked HFB wave functions cannot display time reversal, triaxial or axial symmetry. This loss of symmetry makes the calculations very difficult.

The symmetries preserved by J_x are parity, reflection through yz plane, and rotation of π about the x-axis. Since $\sigma_x = PR_x(\pi)$, only two of these symmetries are independent. If the conventional $|jm\rangle$ basis is used, then the reflection symmetry σ_x does not reduce the dimension of the CHFB equations. This is because J_x is a linear combination of raising and lowering operators, so that J_x is not block diagonal in the quantum number m.

To take advantage of the symmetry σ_x, Goodman[18] introduced a single particle basis that simultaneously block diagonalizes the J_x term and the HF and pair potentials. Since $\sigma_x^2 = -1$ when acting on one-fermion states, the operator σ_x has only two eigenvalues, -i and +i, with corresponding sets of eigenvectors that we denote by $|K>$ and $|\bar{K}>$. Because σ_x and J_x are commuting normal operators, it follows that there are no non-zero matrix elements of J_x between eigenstates of σ_x belonging to different eigen values of σ_x. That is,

$$<K|J_x|\bar{K}> = 0 \qquad \text{(III.5.60)}$$

The eigenvectors are easily determined, since σ_x in the two-dimensional basis $|k\ \bar{k}>$ has the representation

$$\sigma_x = -i \begin{pmatrix} 0 & 1 \\ 1 & 0 \end{pmatrix} \qquad \text{(III.5.61)}$$

so that the eigenvectors are

$$\begin{aligned} |K> &= 2^{-\frac{1}{2}} [\,|k> + |\bar{k}>] \\ |\bar{K}> &= 2^{-\frac{1}{2}} [-|k> + |\bar{k}>] \end{aligned} \qquad \text{(III.5.62)}$$

Notice that $|\bar{K}> = T|K>$. Since J_x and T anticommute it follows that

$$<K|J_x|K'> = -<\bar{K}|J_x|\bar{K}'> \qquad \text{(III.5.63)}$$

eqs. (III.5.60) and (III.5.63) indicate that J_x is block diagonal in the σ_x basis $|K_1\ K_2 \ldots K_N\ \bar{K}_1\ \bar{K}_2 \ldots \bar{K}_N>$:

$$J_x = \begin{pmatrix} j_x & 0 \\ 0 & -j_x \end{pmatrix} \qquad \text{(III.5.64)}$$

If the quasiparticle operators are chosen as

$$q_i^+ = \sum_K (U_{iK}\, a_K^+ + V_{iK}\, a_{\bar{K}})$$

$$q_{\bar{i}}^+ = \sum_K (\bar{U}_{iK}\, a_{\bar{K}}^+ + \bar{V}_{iK}\, a_K)$$

it can then be demonstrated that the CHFB equations reduce to the form

$$\begin{pmatrix} X_1 - \omega j_x & \Delta_1 \\ \Delta_1^+ & -(X_2 + \omega j_x)^* \end{pmatrix} \begin{pmatrix} \vec{U}_i \\ \vec{V}_i \end{pmatrix} = E_i \begin{pmatrix} \vec{U}_i \\ \vec{V}_i \end{pmatrix} \qquad \text{(III.5.65)}$$

$$\begin{pmatrix} (X_2 + \omega j_x)^* & \Delta_1^+ \\ \Delta_1 & -(X_1 - \omega j_x) \end{pmatrix} \begin{pmatrix} \vec{U}_i^* \\ -\vec{V}_i^* \end{pmatrix} = \tilde{E}_i \begin{pmatrix} \vec{U}_i^* \\ -\vec{V}_i^* \end{pmatrix} \qquad \text{(III.5.66)}$$

where X now includes the Fermi energy λ. It is easy to show that

$$\tilde{U}_i = V_i^*, \quad \tilde{V}_i = U_i^* \quad \tilde{E}_i = -E_i \qquad \text{(III.5.67)}$$

So only eq. (III.5.65) need to be solved.

Goodman[18] demonstrated that if the self-consistent symmetry σ_x is employed, the HFB quasiparticle vacuum at any angular velocity may be written as

$$|\phi_o\rangle = \prod_\alpha a_\alpha^+ \prod_{\beta\neq\alpha} (U_\beta + V_\beta\, a_\beta^+ a_{\bar{\beta}}^+)|0\rangle \qquad \text{(III.5.68)}$$

where

$$a_\beta^+ = \sum_K D_{\beta K}\, a_K^+ \qquad \text{(III.5.69)}$$

$$a_{\bar{\beta}}^+ = \sum_K \tilde{D}_{\beta K}\, a_{\bar{K}}^+ \qquad \text{(III.5.70)}$$

so that $|\beta>$ and $|\bar{\beta}>$ are eigenvectors of σ_x with eigenvalues, respectively, of $-i$ and $+i$.

III.5.4 The CHFB calculations in the case of pairing-plus-q.q interactions

We have made the following approximations:

(i) The contribution of the pairing term of the Hamiltonian (III.2.3) is neglected in constructing the potential Γ given by eq. (III.5.32).

(ii) The exchange part of the q.q interaction is also dropped in constructing Γ as well as Δ.

We now give explicit expressions for the matrix elements of Γ as well as Δ in the "σ_x-oriented" basis discussed above.

III.5.5 Matrix Elements of Hartree-Fock Hamiltonian

Let $|K>$ denote a state in the 'direct' basis and $|\bar{K}>$ the state in the 'conjugate' basis; that is

$$|K> = [|j_\alpha m_\alpha> + (-1)^{j_\alpha + \frac{1}{2}} |(j_\alpha, -m_\alpha)>] \equiv |+> \qquad \text{(III.5.71)}$$

$$|\bar{K}> = [|j_\alpha m_\alpha> - (-1)^{j_\alpha + \frac{1}{2}} |(j_\alpha, -m_\alpha)>] \equiv |-> \qquad \text{(III.5.72)}$$

then the matrix elements of the HF potential is

$$\Gamma_{K_1,K_2} = \sum_\beta <K_1, \beta|V|K_2, \beta>$$

$$= \sum_{K_3} \sum_{K_4} <K_1,K_3|V|K_2,K_4> \rho_{K_3,K_4}$$

Denoting the Γ matrix constructed in the K-basis for protons by $\Gamma_{+,p}$ we have

$$\Gamma_{+,p} = \sum_{K_3 K_4} \Big[\langle {}^{p}_{+}\,{}^{p}_{+} | V | {}^{p}_{+}\,{}^{p}_{+} \rangle \rho_{+,p} + \langle {}^{p}_{+}\,{}^{p}_{-} | V | {}^{p}_{+}\,{}^{p}_{-} \rangle \rho_{-,p}$$

$$+ \langle {}^{p}_{+}\,{}^{n}_{+} | V | {}^{p}_{+}\,{}^{n}_{+} \rangle \rho_{+,n} + \langle {}^{p}_{+}\,{}^{n}_{-} | V | {}^{p}_{+}\,{}^{n}_{-} \rangle \rho_{-,n} \Big] \quad \text{(III.5.73)}$$

where p over + (or −) implies 'proton' and n implies 'neutron'.

$$\langle K_1 | \rho_{+,p} | K_2 \rangle = \sum_{\beta} |V_\beta|^2 D^{*}_{\beta K_1} D_{\beta K_2} \quad \text{(III.5.74)}$$

Pairing matrix element

The pairing matrix element is

$$\langle \beta_1, \bar{\beta}_1 | V_p | \beta_2, \bar{\beta}_2 \rangle = \sum_{K_1} D_{\beta_1 K_1} \sum_{K_2} D_{\bar{\beta}_1 K_2} \sum_{K_3} D_{\beta_2 K_3} \sum_{K_4} D_{\bar{\beta}_2 K_4}$$

$$\langle K_1 \bar{K}_2 | V_p | K_3 \bar{K}_4 \rangle \quad \text{(III.5.75)}$$

The matrix elements of the pairing interaction are given by

$$\langle j_1 m_1 , j_2 m_2 | V_p | j_3 m_3 , j_4 m_4 \rangle = (-G)(-1)^{j_1 + j_3 - m_1 - m_3}$$

$$\delta_{j_1 j_2} \delta_{j_3 j_4} \delta_{m_2, -m_1} \delta_{m_4, -m_3} \cdot \quad \text{(III.5.76)}$$

Employing eq. (III.5.76) we obtain, after some algebraic manipulations

$$\langle \beta_1 \bar{\beta}_1 | V_p | \beta_2 \bar{\beta}_2 \rangle = - G \Big(\sum_{K_1} D_{\beta_1 K_1} D_{\bar{\beta}_1 K_1} (-1)^{l_\alpha} \Big) \times$$

$$\Big(\sum_{K_2} D_{\beta_2 K_2} D_{\bar{\beta}_2 \bar{K}_2} (-1)^{l_\alpha} \Big)$$

where $|K_1\rangle$ is given by eq. (III.5.71)

III.6.1 CHFB results for the doubly even Molybdenum isotopes in the ($3s_{1/2}$, $2d_{3/2}$, $2d_{5/2}$, $1g_{7/2}$, $1g_{9/2}$, $1h_{11/2}$) space

In this section we present the HFB as well as the CHFB results for the nuclei $^{92-104}$Mo.

The choice of the valence space as well as the inert core is the same as in our earlier CHF calculations. The strengths of the various components of the pairing - plus - quadrupole-quadrupole interaction are:

$$\chi_{nn} \ (=\chi_{pp}) = -0.016 \text{ MeV b}^{-4}, \quad \chi_{np} = -0.0352 \text{ MeV b}^{-4}$$

and $G_p = 0.18$ MeV.

Table III.6 summarizes the HFB results for the Mo isotopes. A comparison of these results with the ones given in the Table III.2 brings out the role of the like-particle pairing correlations. It turns out that the $<Q_o^2>_{HFB}$ values are only marginally different from the $<Q_o^2>_{HF}$ values given earlier. The calculation emphasizes the role of the $1h_{11/2}$ orbit in the context of the onset of large deformations; the $1h_{11/2}$ occupation numbers for the deformed nuclei $^{100-104}$Mo are 2.01, 3.86 and 4.59 respectively. The $2d_{5/2}$ occupation numbers, which are in fact slightly smaller than their HF values, further underscore the result that the occurrence of large deformations in this region is <u>not</u> compatible with the usual assumption of an inert ^{94}Sr (Z=38, N=56) core.

The CHFB spectra for the nuclei ^{104,106}Mo have been given in figure 4. The present calculation reproduces

e calculated values of the intrinsic quadrupole moments as well as the sub-shell occupancies for the B states in the doubly-even Mo isotopes. Here $\langle Q_o^2 \rangle_p$ ($\langle Q_o^2 \rangle_n$) gives the contribution of the protons eutrons) to the intrinsic quadrupole moments.

otope	$\langle Q_o^2 \rangle$ ($\langle Q_o^2 \rangle_p$, $\langle Q_o^2 \rangle_n$)	$\langle Q_o^2 \rangle_{max}$	Sub-shell occupancy											
			Neutrons						Protons					
			$3s_{1/2}$	$2d_{3/2}$	$2d_{5/2}$	$1g_{7/2}$	$1g_{9/2}$	$1h_{11/2}$	$3s_{1/2}$	$2d_{3/2}$	$2d_{5/2}$	$1g_{7/2}$	$1g_{9/2}$	$1h_{11/2}$
^{2}Mo	8.6 (4.9, 3.7)	63.6	0.00	0.00	0.07	0.00	9.92	0.00	0.00	0.00	0.03	0.00	1.91	0.05
^{4}Mo	32.3 (11.8, 20.5)	67.6	0.63	0.44	1.13	0.15	9.65	0.00	0.06	0.02	0.40	0.00	1.57	0.06
^{6}Mo	42.0 (12.9, 29.1)	71.6	0.68	1.03	1.82	1.02	9.48	0.04	0.11	0.04	0.55	0.02	1.26	0.00
^{8}Mo	45.5 (13.4, 32.1)	75.6	0.69	1.36	2.59	1.56	9.79	0.00	0.13	0.06	0.59	0.01	1.19	0.00
^{0}Mo	53.5 (14.1, 39.4)	78.7	0.73	1.38	2.43	1.78	9.66	2.01	0.18	0.09	0.67	0.03	1.02	0.00
^{2}Mo	59.4 (14.5, 44.9)	78.6	0.74	1.39	2.39	1.94	9.67	3.86	0.21	0.12	0.71	0.04	0.92	0.00
^{4}Mo	60.4 (14.6, 45.8)	76.6	0.75	1.42	2.98	2.56	9.70	4.59	0.21	0.12	0.71	0.04	0.90	0.00

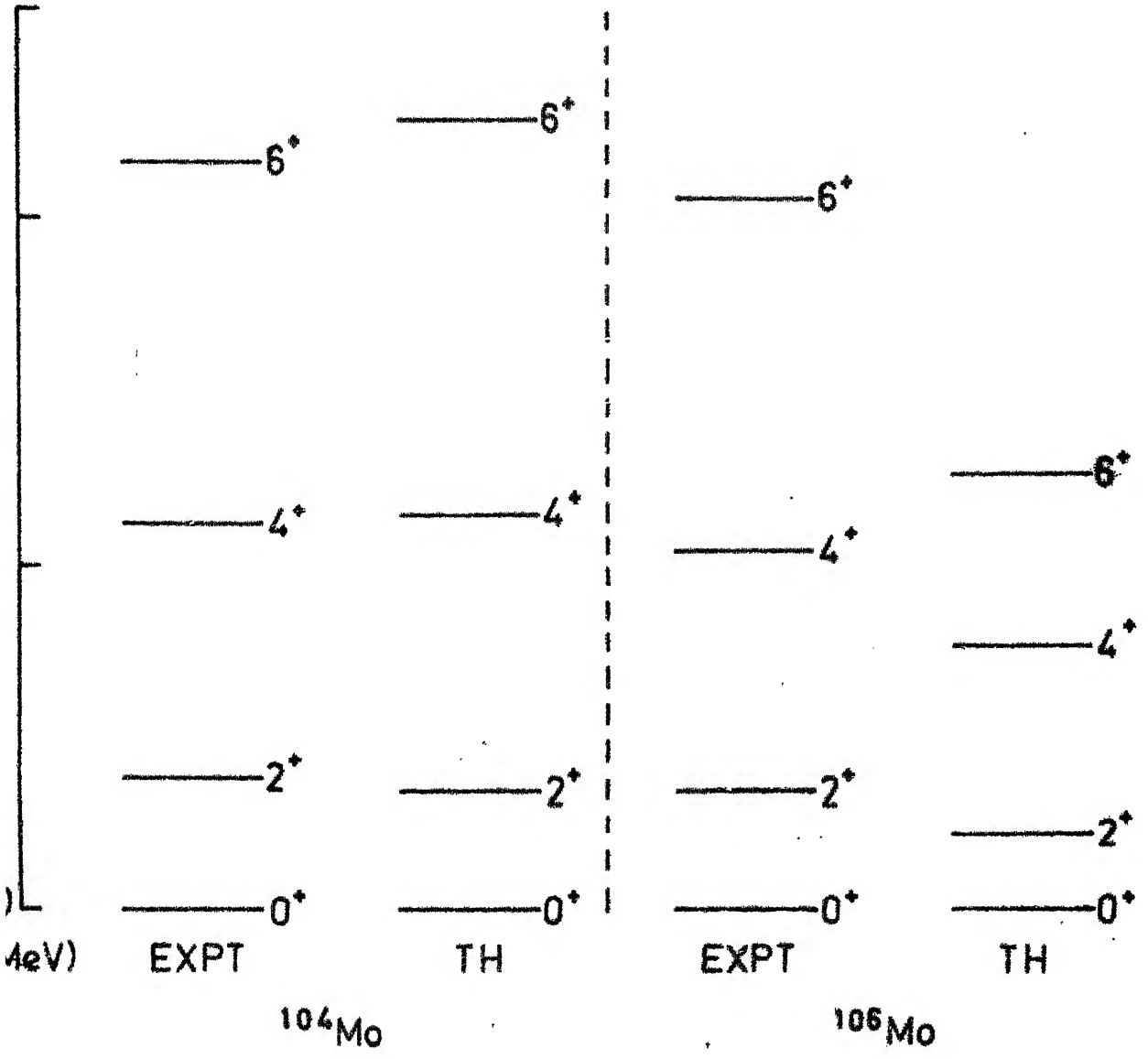

Fig. 4. Comparison of the calculated and the experimental yrast spectra in the nuclei ^{104}Mo and ^{106}Mo.

TABLE III.7

Details of ^{104}Mo wavefunctions. The occupation probabilities v_α^2 as well as the pairing gaps $\Delta_{\alpha\bar{\alpha}}$ are given for four neutrons pairs near the Fermi surface for the various yrast levels. Here ω denotes the cranking frequency required to obtain the various J's. For each J the states α are ordered with decreasing v_α^2.

J^π	ω	$\langle J_x \rangle$	α	v_α^2	$\Delta_{\alpha\bar{\alpha}}$(MeV)
2^+	0.1129	2.444	1	0.984	0.51
			2	0.958	0.54
			3	0.607	0.53
			4	0.306	0.50
4^+	0.1789	4.467	1	0.984	0.50
			2	0.962	0.53
			3	0.622	0.52
			4	0.286	0.49
6^+	0.2467	6.481	1	0.986	0.49
			2	0.967	0.52
			3	0.652	0.51
			4	0.254	0.48

TABLE III.8

Details of ^{106}Mo wavefunctions. For further comments, see Table III.7.

J^π	ω	$\langle J_x \rangle$	α	V_α^2	$\Delta_{\alpha\bar{\alpha}}$ (MeV)
2^+	0.1223	2.446	1	0.986	0.45
			2	0.915	0.48
			3	0.834	0.43
			4	0.195	0.47
4^+	0.1923	4.478	1	0.987	0.45
			2	0.928	0.47
			3	0.812	0.42
			4	0.202	0.46
6^+	0.2630	6.483	1	0.988	0.45
			2	0.939	0.46
			3	0.789	0.42
			4	0.204	0.45

successfully the yrast spectrum in ^{104}Mo. The computed yrast spectrum in ^{106}Mo is, however, found quite compressed compare to the observed one. In Tables III.7 and III.8 we have presented some of the details of the yrast levels in the nucl ^{104,106}Mo. A close scrutiny of the V_α^2 values reveals a smal but systematic reduction in the pairing correlations in going from $J^\pi = 2^+$ to $J^\pi = 6^+$ in ^{104}Mo.

III.6.2 CHFB calculations for the doubly even Zirconium isotopes in the $(2p_{1/2}, 3s_{1/2}, 2d_{3/2}, 2d_{5/2}, 1g_{7/2}, 1g_{9/2}, 1h_{11/2})$ space

We present here first the HFB results for the doubly even Zr isotopes. The valence space includes, in addition to the orbits employed in the calculations just discussed, also the orbital $2p_{1/2}$. The strength parameters characterizing the effective interaction are: $\chi_{nn}(=\chi_{pp})=-0.01$ MeV b^{-4}, $\chi_{np} = -0.0231$ MeV b^{-4} and $G_p = 0.18$ MeV. In addition to the SPE's quoted in section III.2, we have used $\epsilon(2p_{1/2}) = -0.8$ MeV.

In Table III.9 we present the intrinsic quadrupole deformations as well as the sub-shell occupancies for the intrinsic HFB states in the nuclei $^{94-102}$Zr. It is seen that the results are not qualitatively different from the ones obtained from the HF picture. The calculation reproduces the sudden onset of deformations in going from the nucleus ^{98}Zr to ^{100}Zr; whereas the intrinsic HFB quadrupole moment in ^{98}Zr is only 39.3b^2 out of a maximum of 76.7 b^2, that

The calculated values of the quadrupole moments as well as the sub-shell occupancies for the HFB intrinsic states in the highly neutron-rich Zr isotopes.

X	$\frac{\langle Q_o^2 \rangle}{[\langle Q_o^2\rangle_p, \langle Q_o^2\rangle_n]}$	$\langle Q_o^2\rangle_{max}$	Sub-shell occupancy													
			Neutrons							Protons						
			$3s_{1/2}$	$2p_{1/2}$	$2d_{3/2}$	$2d_{5/2}$	$1g_{7/2}$	$1g_{9/2}$	$1h_{11/2}$	$3s_{1/2}$	$2p_{1/2}$	$2d_{3/2}$	$2d_{5/2}$	$1g_{7/2}$	$1g_{9/}$
Zr	$\frac{24.8}{[7.5, 17.3]}$	73.4	0.54	2.00	0.26	3.04	0.10	9.96	0.09	0.02	0.07	0.00	0.13	0.03	1.75
Zr	$\frac{07.7}{[2.0, 5.7]}$	77.7	0.65	1.99	0.14	4.94	0.17	9.96	0.11	0.05	0.92	0.01	0.02	0.01	0.99
Zr	$\frac{39.3}{[10.8, 28.5]}$	76.7	0.74	1.99	1.29	3.69	1.36	9.90	1.02	0.04	0.00	0.01	0.32	0.00	1.62
Zr	$\frac{48.4}{[12.8, 35.6]}$	75.4	0.77	1.99	1.40	3.46	1.98	9.94	2.46	0.10	0.00	0.04	0.53	0.13	1.29
Zr	$\frac{44.8}{[11.5, 33.3]}$	73.8	0.96	1.99	1.48	4.25	2.44	9.89	2.99	0.06	0.00	0.02	0.39	0.01	1.52

for ^{100}Zr is approximately 64 per cent of the maximum possible value for the given space.

In figure 5 we have displayed the sub-shell occupation numbers for the various orbits that we have calculated by employing the HFB intrinsic states for the nuclei $^{94-102}Zr$. The observed spectrum (see Fig. 1) in ^{96}Zr is characterized by a rather large ($\sim$1.76 MeV) value of the $(E_2+ - E_0+)$ separation. It is reasonable to interpret this feature in terms of the $2d_{5/2}$ sub-shell closure. The computed values for the $2d_{5/2}$ occupation numbers are, in fact, seen to display this effect.

The computed values for the $1h_{11/2}$ occupancies bring out the strong correlation between the increased occupation of this level and the sudden onset of large deformations in $^{100,102}Zr$. Further, the present results indicate that the onset of deformations is also marked by a significant depletion of the $2d_{5/2}$ orbit; the sub-shell occupation number for this orbit in ^{100}Zr is only 3.46. This invalidates the usual assumption concerning the inertness of ^{94}Sr core which has formed the basis of the earlier investigations[4-6] regarding the origin of deformations in the Zirconium region.

Federman and Pittel[5] have earlier conjectured that the occurrence of deformations in $^{100,102}Zr$ may be arising primarily from the $[(1g_{9/2})_p - (1g_{7/2})_n]$ effective interaction. This mechanism demands a correlation between the $1g_{9/2}$-proton and $1g_{7/2}$ -neutron occupation numbers. In view of the small

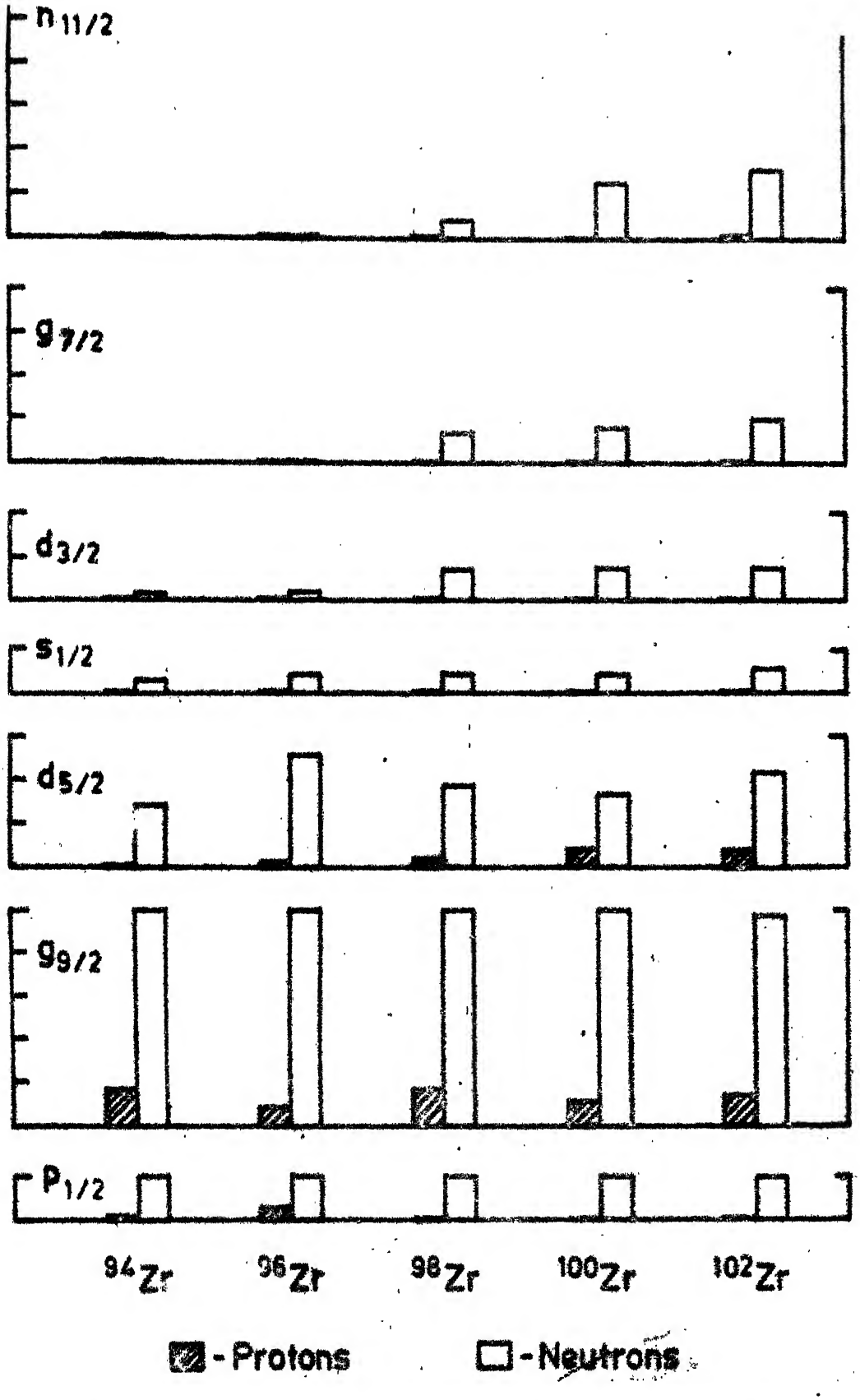

Fig. 5. Subshell occupation numbers for protons and neutrons in the ground states of doubly even Zr isotopes.

computed values of the $1g_{7/2}$ occupation numbers - the values are seen to range only between 1.36 and 2.44 in the nuclei $^{98-102}Zr$ - the present calculation does not support this idea.

Table III.10 summarizes our HFB results for the isotopes $^{92-106}Mo$. The computed $\langle Q_o^2 \rangle_{HFB}$ values are quite consistent with the observed deformation trends (see Fig. 1(b)). The $(E_{2^+} - E_{0^+})$ separations in the nuclei $^{104,106}Mo$ are 0.19 MeV and 0.17 MeV respectively; this is to be contrasted with the value 1.51 MeV for this separation in the nearly-spherical nucleus ^{92}Mo. The present HFB calculation yields intrinsic deformations for the nuclei $^{104,106}Mo$ which are about 96 percen of the respective $\langle Q_o^2 \rangle_{max}$ values.

A consideration of the $1h_{11/2}$ occupation numbers again reveals the connection between them and the onset of large deformations in Mo isotopes. Further an examination of the $1g_{9/2}$-proton and the $1g_{7/2}$-neutron occupation numbers also fails to suggest any increased involvement of the $[(1g_{9/2})_p - (1g_{7/2})_n]$ effective interactions in the quasirotational isotopes $^{100-106}Mo$.

In figure 6 we present the CHFB yrast spectra for the nuclei $^{100,102}Zr$. In ^{100}Zr the calculated $(E_{6^+} - E_{4^+})$ value is about 0.5 MeV too large compared with the experiments. The yrast spectrum in ^{102}Zr is, however, in fair agreement with the observed one.

TABLE III.10

The quadrupole moments as well as the sub-shell occupancies for the HFB intrinsic st
in some highly neutron rich Mo isotopes.

$\langle Q_o^2 \rangle$ / $\langle Q_o^2 \rangle_p, \langle Q_o^2 \rangle_n$	$\langle Q_o^2 \rangle_{max}$	Sub-shell occupancy													
		Neutrons							Protons						
		$3s_{1/2}$	$2p_{1/2}$	$2d_{3/2}$	$2d_{5/2}$	$1g_{7/2}$	$1g_{9/2}$	$1h_{11/2}$	$3s_{1/2}$	$2p_{1/2}$	$2d_{3/2}$	$2d_{5/2}$	$1g_{7/2}$	$1g_{9/2}$	
13.9 [8.6,5.3]	77.9	0.00	2.00	0.00	0.15	0.01	9.84	0.00	0.00	1.08	0.00	0.08	0.02	2.82	C
34.8 [16.1,18.7]	80.6	0.62	2.00	0.31	1.20	0.09	9.78	0.00	0.02	0.02	0.01	0.35	0.02	3.58	C
42.3 [17.7,24.6]	84.8	0.64	1.99	0.83	2.15	0.62	9.77	0.00	0.03	0.00	0.01	0.47	0.01	3.47	C
49.4 [18.9,30.5]	88.9	0.66	1.99	1.31	2.91	1.26	9.87	0.00	0.06	0.00	0.02	0.61	0.02	3.29	C
80.5 [24.7,55.8]	87.9	0.83	2.00	1.40	1.96	2.53	7.27	4.01	0.29	0.00	0.27	1.30	0.19	1.95	C
84.6 [25.1,59.5]	86.9	0.86	2.00	1.40	1.93	2.70	7.10	6.00	0.32	0.00	0.33	1.35	0.24	1.76	C
82.9 [25.1,57.8]	86.2	0.86	2.00	1.44	3.12	3.18	7.40	6.00	0.32	0.00	0.33	1.34	0.24	1.77	0
82.1 [25.1,56.9]	84.5	0.88	1.99	1.64	3.28	3.43	7.47	7.28	0.32	0.00	0.32	1.34	0.24	1.70	0

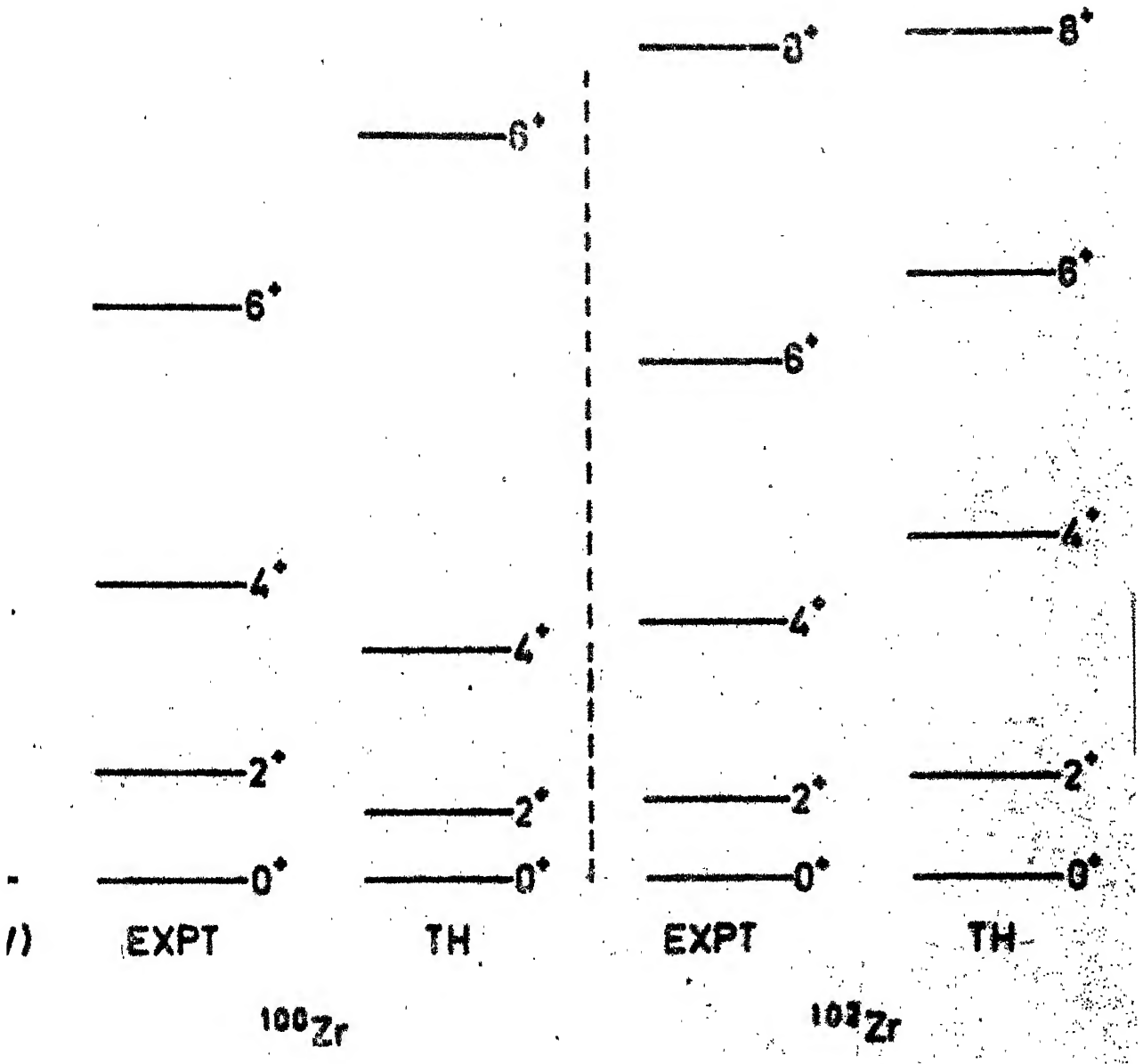

6. Comparison of the calculated and the experimental yrast spectra in the nuclei ^{100}Zr and ^{102}Zr.

TABLE III.11

Details of ^{100}Zr wavefunctions. The last column gives the contribution to the angular momentum, $J_\alpha = \left[\langle J_x \rangle_{\alpha\alpha} + \langle J_x \rangle_{\bar{\alpha}\bar{\alpha}}\right] V_\alpha^2$, for various orbits α.

J^π	ω	$\langle J_x \rangle$	α	V_α^2	$\Delta_{\alpha\bar{\alpha}}$ (MeV)	J_α
			1	0.957	0.87	0.11
			2	0.797	0.86	10.01
2^+	0.1480	2.451	3	0.376	0.85	0.74
			4	0.297	0.86	1.99
			5	0.214	0.87	-0.38
			1	0.952	0.88	0.66
			2	0.824	0.85	10.25
4^+	0.1880	4.765	3	0.360	0.85	1.02
			4	0.267	0.84	3.04
			5	0.227	0.85	-0.42
			1	0.954	0.86	0.36
			2	0.859	0.83	10.33
6^+	0.217	6.490	3	0.366	0.85	1.00
			4	0.281	0.83	3.54
			5	0.225	0.85	-0.44

TABLE III.12

Details of ^{102}Zr wavefunctions

J^π	ω	$\langle J_x \rangle$	α	V_α^2	$\Delta_{\alpha\bar{\alpha}}$ (MeV)	J_α
			1	0.957	1.00	1.63
			2	0.831	0.97	9.94
2^+	0.1310	2.43	3	0.578	0.98	0.81
			4	0.469	0.98	1.73
			5	0.441	1.00	-0.27
			1	0.957	1.00	1.07
			2	0.858	0.96	10.04
4^+	0.1620	4.466	3	0.574	0.97	0.83
			4	0.485	0.97	2.49
			5	0.436	0.99	-0.18
			1	0.956	0.99	0.860
			2	0.873	0.95	10.02
6^+	0.1965	6.500	3	0.556	0.95	0.02
			4	0.512	0.96	3.14
			5	0.457	0.97	-0.00
			1	0.956	0.98	0.77
			2	0.897	0.93	10.18
8^+	0.2320	8.490	3	0.553	0.94	0.88
			4	0.529	0.94	3.66
			5	0.451	0.96	-0.04

In Tables III.11 and III.12 we present some of the details of the CHFB wavefunctions for the yrast levels in $^{100,102}Zr$. The non-axial orbits of $1h_{11/2}$ parentage can easily be identified here through their relatively large ($\sim$10.0) contributions towards $\langle J_x \rangle$. The occupation probabilities for the non-axial $h_{11/2,\alpha}$ orbits show a systematic increase in going from the $J^\pi = 2^+$ to $J^\pi = 6^+$ members of the yrast cascade in the nuclei $^{100,102}Zr$.

III.7 Conclusions

The purpose of the present investigation was to examine, in a microscopic manner, the origin of the dramatic onset of large deformation in the Zirconium region. Some recen investigations[6] have attempted to established a link between the occurrence of large deformations in the region with the simultaneous occupation of neutrons and protons of the spin-orbit partner orbits $1g_{7/2}$ and $1g_{9/2}$. In view of the calculations presented here, the earlier result appears to be an artefact of the model employed; the earlier calculations involv an inert ^{94}Sr core with the protons confined to the orbits $2p_{1/2}$, $1g_{9/2}$ and $2d_{5/2}$ and the neutrons to the $3s_{1/2}$, $2d_{3/2}$ $1g_{7/2}$ and $1h_{11/2}$ orbits. The following conclusions can be drawn from the HFB (as well as some CHFB) results obtained in the present work:

(i) The involvement of the $1h_{11/2}$ orbit is one of the most important factors responsible for the observed dramatic onset of large deformations at N=60.

(ii) The observed large deformations in the Zirconium region imply a significant polarization of the ^{94}Sr core. In other words, the assumption of an inert ^{94}Sr core is not consistent with the observed rotational features in the doubly even isotopes of Zirconium and Molybdenum with A>100.

(iii) The calculations do not reveal any significant connection between the occurrence of deformations in this region and the selective occupation of the $(1g_{9/2})$-proton and the $(1g_{7/2})$-neutron orbits.

REFERENCES

1. E. Cheifetz, R.C. Jared, S.G. Thompson and J.B. Wilhelmy, Phys. Rev. Lett. 25 (1970) 38.
2. N. Auerbach and I. Talmi, Nuclear Phys. 64 (1965) 458.
3. D.H. Gloeckner, Nucl. Phys. 253A (1975) 301.
4. P. Federman and S. Pittel, Phys. Lett. 69B (1977) 385
5. P. Federman and S. Pittel, Phys. Lett. 77B (1978) 29.
6. P. Federman, S. Pittel and R. Campos, Phys. Lett. 82B (1979) 9.
7. P. Federman and S. Pittel, Phys. Rev. C20 (1979) 820.
8. J.D. Vergados and T.T.S. Kuo, Phys. Lett. 35B (1971) 93.
9. M. Baranger and K. Kumar, Nucl. Phys. A110 (1968) 490.
10. R. Beck, H.J. Mang and P. Ring, Z. Physik 231, (1970) 10.
11. F.M.H. Villars and N. Schmeing-Rogerson, Ann. Phys.(NY) 63 (1971) 443.
12. S.K. Sharma, L. Satpathy, S.B. Khadkikar and S.C.K. Nair, Phys. Letters 61B (1976) 122.
13. C.R. Bingham and M.L. Halbert, Phys. Rev. C2 (1970) 2297.
14. Alan L. Goodman, in Advances in Nuclear Physics, Volume 11, Plenum Press New York (1979).
15. D. Inglis, Phys. Rev. 96 (1954) 1059.
16. D. Inglis, Phys. Rev. 103 (1956) 1786.
17. H.J. Mang, Phys. Reports 18 (1975) 325.
18. A. Goodman, Nuclear Phys. A230 (1974) 466.

CHAPTER IV

MICROSCOPIC DESCRIPTION OF THE YRAST AND THE YRARE BANDS IN ^{100}Pd AND ^{102}Pd

IV.1 Introduction

Scharff-Goldhaber *et al.*[1] have some time ago reported the level schemes of the nuclei ^{100}Pd (N=54, Z=46) and ^{102}Pd (N=56, Z=46) populated by heavy-ion induced reactions. The levels in ^{100}Pd were populated in the ^{91}Zr (^{12}C, 3n) and the ^{90}Zr (^{13}C, 3n) reactions. The spectra in ^{102}Pd were obtained through the ^{92}Zr (^{13}C, 3n) and ^{94}Zr (^{12}C, 4n) reactions.

The observed yrast as well as the yrare spectra in the nuclei ^{100,102}Pd are marked by considerable departures from the rotational behaviour (see Fig. 7). The yrast band in ^{100}Pd (J_{max}=14) was found to deviate significantly from the "variable moment of inertia" (VMI) predictions[2]. The levels of the yrare band with $J^{\pi} \geq 8^{+}$ also displayed similar properties. The yrare band in ^{100}Pd also had J_{max} = 14 and an experimental search for the low-spin members (with J<8) of this band had proved inconclusive. The yrast band in ^{102}Pd, reaching J=14, was found to deviate only slightly from the VMI predictions. However, the available yrare states in ^{102}Pd with J^{π} =10^{+}, 12^{+} and 14^{+} showed significant deviations from even the VMI law.

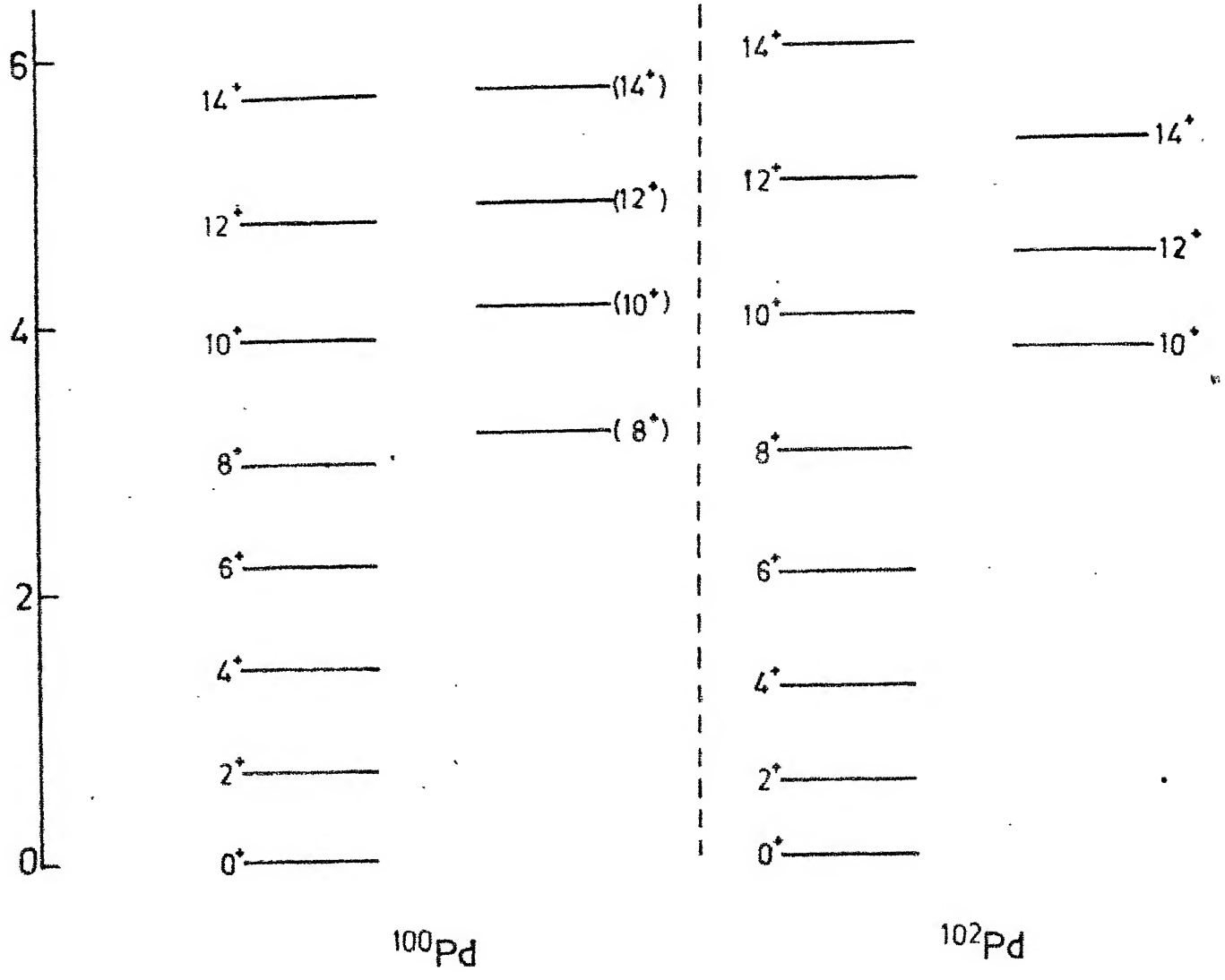

Fig. 7. Observed level schemes for the nuclei $^{100,102}Pd$.

The earlier phenomenological attempts[2,3] at understanding the observed levels in ^{100,102}Pd have met with limited success. Apart from the earlier studies in the framework of the VMI model, an attempt was also made by Smith and Volkov[3] to explain the observed featuresof the yrast and the yrare bands in the Palladium isotopes by invoking instability towards asymmetric deformations at sufficiently high (>8) angular momenta.[3] However a lack of any microscopic calculation has hindered an understanding of the observed spectra in terms of the underlying single-particle states.

In this chapter we carry out a microscopic study of the yrast and the yrare bands in the nuclei ^{100,102}Pd by employing the variation-after-projection (VAP) formalism[4] in conjunction with the HFB ansatz for the axially symmetric intrinsic wavefunctions. The choice of the VAP method was dictated by two considerations. Firstly, it is desirable to use a calculationa framework which allows for the possibility of having different intrinsic states for each yrast level, in view of the observed large deviations of the yrast levels in these isotopes from the J(J+1)-law. Secondly it is rather easy to compute the intra-band E2 transition probabilities in the VAP method. In the present work we have again used the pairing-plus-quadrupole quadrupole effective interaction operating in the 3s-2d-1g-1h_{11} configuration space.

The results presented in this chapter bring out the significant role played by the $1h_{11/2}$ orbit in lending a

somewhat dichotomic character to the yrast spectra in the nuclei ^{100,102}Pd; it turns out that the yrast spectra can be interpreted in terms of two intrinsic states occurring at about the same energy but possessing different sub-shell occupancies for the $1h_{11/2}$ orbit.

In section IV.2 we discuss the method of calculation. The procedure for obtaining axially symmetric HFB intrinsic states (with $K = \langle J_z \rangle = 0$) is already contained in our earlier discussion of the CHFB method that we have presented in the preceding chapter. We have, therefore, confined ourselves to only a brief outline of the technique of exact angular momentum projection from HFB intrinsic states. In section IV.3 we present and discuss our VAP results. Finally, section IV.4 contains some concluding remarks.

IV.2 Calculational framework

IV.2.1 Angular momentum projection from HFB intrinsic states

For axially symmetric HFB intrinsic states (with K=0) the states $|\alpha\rangle$ appearing in (III.5.51) can be labelled by their 'm' values, where $m = \langle j_z \rangle$. Thus the HFB state can be written as[5]

$$|\Phi_o\rangle = \prod_{im} (U_{im} + V_{im}\, a^+_{im}\, a^+_{i\bar{m}})|0\rangle \qquad \text{(IV.2.1)}$$

Here 'i' labels the different deformed orbits with the same value of m.

The creation operators a^+_{im} can be written as

$$a^+_{im} = \sum_j D_{im,j}\, a^+_{jm} \; ; \; a^+_{i\bar{m}} = \sum_j (-1)^{1+j-m} D_{im,j}\, a^+_{j-m} \qquad \text{(IV.2.2)}$$

Here j labels the spherical single-particle orbits $1g_{9/2}$, $2d_{5/2}$, $3s_{1/2}$, $2d_{3/2}$, $1g_{7/2}$, $1h_{11/2}$.

The wavefunction expressed in (IV.2.1) can be recast into the form

$$|\Phi_o> = N \exp\left(\frac{1}{2} \sum_{\alpha\beta} f_{\alpha\beta}\, a^+_\alpha a^+_\beta\right)|0> \qquad \text{(IV.2.3)}$$

with

$$f_{\alpha\beta} = \sum_i D_{im_\alpha, j_\alpha} D_{im_\beta, j_\beta} (V_{im_\alpha}/U_{im_\alpha})\, \delta_{m_\alpha, -m_\beta} \qquad \text{(IV.2.4)}$$

Here we have denoted the quantum numbers $(j_\alpha\ m_\alpha)$ by α, and N is a normalization constant.

Writing the shell-model Hamiltonian (III.5.1)

as

$$H = \sum_\alpha \varepsilon_\alpha a^+_\alpha a_\alpha + \frac{1}{4} \sum_{\alpha\beta\gamma\delta} <\alpha\beta|V_A|\gamma\delta> a^+_\alpha a^+_\beta a_\delta a_\gamma$$

we can write the energy of a state with angular momentum J as

$$E_J = <\Phi_o|H P^J_{oo}|\Phi_o>/<\Phi_o|P^J_{oo}|\Phi_o>$$
$$= \left(\int_o^\pi h(\theta)\, d^J_{oo}(\theta)\, \mathrm{Sin}\theta d\theta\right)/\left(\int_o^\pi n(\theta)\, d^J_{oo}(\theta)\, \mathrm{Sin}\,\theta\, d\theta\right) \qquad \text{(IV.2.5)}$$

The intensities of the various angular momenta contained in the intrinsic wavefunction are given by

$$a^2_J = \frac{1}{2}(2J+1) \int_o^\pi n(\theta)\, d^J_{oo}(\theta)\, \mathrm{Sin}\,\theta\, d\,\theta \qquad \text{(IV.2.6)}$$

The overlap integrals $h(\theta)$ and $n(\theta)$ are given by

$$h(\theta) = n(\theta)\Big[\sum_\alpha \varepsilon_\alpha (M/(1+M))_{\alpha\alpha} + (1/4) \sum_{\alpha\beta\gamma\delta} <\alpha\beta|V_A|\gamma\delta>\cdot$$
$$\{2(M/(1+M))_{\gamma\alpha} (M/(1+M))_{\delta\beta} + \sum_{\nu\rho} (1/1+M)_{\gamma\rho} F_{\rho\delta} (1/(1+M))_{\nu\alpha} f^*_{\nu\beta}\}\Big] \qquad \text{(IV.2.7)}$$

$$n(\theta) = [\det\,(1 + M(\theta))]^{1/2} \qquad \text{(IV.2.8)}$$

Here,

$$F_{\alpha\beta}(\theta) = \sum_{m'_\alpha, m'_\beta} d^{j_\alpha}_{m_\alpha m'_\alpha}(\theta)\; d^{j_\beta}_{m_\beta m'_\beta}(\theta)\; f_{j_\alpha m'_\alpha, j_\beta m'_\beta} \qquad \text{(IV.2.9)}$$

$$M = F\, f^{+} \qquad \text{(IV.2.10)}$$

Employing the angular momentum projected wavefunctions $|\psi^J_{MK}\rangle = P^J_{MK}\,|\phi_o\rangle$ one can write

$$\langle\psi^J_{MK}|Q^2_o|\psi^{J'}_{MK}\rangle = \tfrac{1}{2}\,(2J+1)\sqrt{\tfrac{2}{7}}\,\left[n^J\, n^{J'}\right]^{\frac{1}{2}} \int_0^\pi \sum_\mu \begin{bmatrix} J & 2 & J' \\ -\mu & \mu & 0 \end{bmatrix} d^J_{\mu 0}(\theta)\; n(\theta)$$

$$\times\, b^2 \Big(\sum_{\tau_3 \alpha\beta} e_{\tau 3} \langle\alpha|Q^2_\mu|\beta\rangle\; \rho^{\tau_3}_{\alpha\beta}(\theta)\Big)\, \sin\theta\; d\theta \qquad \text{(IV.2.11)}$$

The static quadrupole moments as well as the E2 transition matrix elements, $B(E2;\, J^+_i \to J^+_f)$, can easily be obtained by using the above relation. Here b is the oscillator length parameter and $Q^2_\mu = (16\pi/5)^{1/2}\,(r^2/b^2)\,Y^2_\mu(\Omega)$. The matrix ρ appearing in eq. (IV.2.11) is defined as

$$\rho = M/(1+M) \qquad \text{(IV.2.12)}$$

Further, the normalizations n^J are given as

$$n^J = \int_0^\pi n(\theta)\; d^J_{00}(\theta)\; \sin\theta\, d\theta \qquad \text{(IV.2.13)}$$

The method of performing the projection calculation is as follows. Employing the HFB wavefunctions we first set up the f matrix. Then F, M and $1/(1+M)$ are evaluated for twenty values of the gaussian quadrature points between the range $(0, \pi/2)$. (The axial symmetry of the intrinsic state permits us to change the integration limits to $(0, \pi/2)$).

The projected energies are then computed from the expressions (IV.2.5 - IV.2.10).

IV.2.2 The Variation-after-projection (VAP) method for studying the yrast spectra

The VAP calculations have been carried out by employing the following procedure. We first generate self-consistent HFB solutions, $\Phi(\beta)$, by carrying out HFB calculatio with the Hamiltonian $(H - \beta Q_o^2)$. The intrinsic state for each yrast level is then selected by finding out the minimum of the projected energy $E_J(\beta)$ $(= \langle \Phi(\beta) | H P^J_{oo} | \Phi(\beta) \rangle / \langle \Phi(\beta) | P^J_{oo} | \Phi(\beta) \rangle)$ as a function of β. In other words, the intrinsic state for each J satisfies the following condition.

$$\delta \left[\langle \Phi(\beta) | H P^J_{oo} | \Phi(\beta) \rangle / \langle \Phi(\beta) | P^J_{oo} | \Phi(\beta) \rangle \right] = 0 \qquad \text{(IV.2.14)}$$

IV.3 Results and discussion

The spherical SPE's that we have employed in the present calculation are (in MeV): $\epsilon(1g_{9/2}) = 0.5$, $\epsilon(2d_{5/2})=5.4$, $\epsilon(3s_{1/2}) = 6.4$, $\epsilon(2d_{3/2}) = 7.9$, $\epsilon(1g_{7/2}) = 8.4$ and $\epsilon(1h_{11/2})=8.$ The strengths of the various components of the pairing-plus-quadrupole-quadrupole interaction were taken as: χ_{nn} $(=\chi_{pp})$ $= -0.012$ MeV b^{-4}, $\chi_{np} = -0.02265$ MeV b^{-4} and $G_p = 0.18$ MeV. The present set of input parameters differs slightly from the earlier one employed in the CHFB calculation for the Molybdenum isotopes. We have reduced the $(1h_{11/2}$-$1g_{9/2}$ separation by 1.1 MeV. Further, the strengths χ's have been reduced by about 25 percent. The lowering of the $1h_{11/2}$ energy is intended to mock up, at least partially, the effects

due to the neglected, higher-lying single-particle orbits.

In tables IV.1 and IV.2 we have given the details of our PHFB as well as VAP calculations for ^{100,102}Pd.

The minimum-energy HFB solutions for ^{100,102}Pd are characterized by large intrinsic quadrupole moments (about $54b^2$ and $66b^2$ respectively). This is consistent with the experiments of L. Hasselgren *et al.*[6] which yield some indications concerning the prolate shapes in the Palladium isotopes with A=102-106.

A comparison of the VAP as well as the PHFB results presented in the table IV.1 reveals a significant change in the yrast spectrum in ^{100}Pd at J=2 - the intrinsic quadrupole moments increases from 54.1 b^2 to 67.3 b^2. The results for the sub-shell occupation numbers indicate that the increase in the deformation is correlated with a noticeable increase in the $1h_{11/2}$-neutron occupation at the cost of the neutrons in the $1g_{9/2}$ orbit.

The VAP results for the nucleus ^{102}Pd (see table IV.2) indicate a significant change of the intrinsic state in going from the yrast J=4 to J=6. Here again a change in the intrinsic deformation of the yrast cascade is accompanied with an enhanced (neutron) occupation of the $1h_{11/2}$ orbit and a depletion of the $1g_{9/2}$ neutrons. The changes occurring in the $\langle Q_o^2 \rangle$ values of the yrast levels in ^{100,102}Pd are roughly equivalent to an increase of the effective Nilsson deformation [illegible] (see figure 2)

Some of the details of the PHFB as well as the VAP calculations in ^{100}Pd. Here E_J(PHFB) gives the projected energies obtained from the eq. (IV.2.5) for the minimum-energy HFB solution. The parameter β_J gives the J-dependent deformations needed to satisfy the VAP equation (IV.2.14). The intrinsic quadrupole moments, projected energies as well as the sub-shell occupations for the various intrinsic states involved in the VAP calculation are also given.

J^π	E_J(PHFB)	VAP								
		β_J	$\langle\Phi(\beta_J)\|Q_0^2\|\Phi(\beta_J)\rangle$	E_J(VAP)	Occupation Probabilities (Neutrons)					
					1/2	3/2	5/2	7/2	9/2	11/2
0^+	15.48	0.00	54.1	15.48	0.67	1.02	1.97	1.03	9.00	0.29
2^+	15.93	0.00	54.1	15.93	0.67	1.02	1.97	1.03	9.00	0.29
4^+	16.88	0.035	67.3	16.74	0.72	1.19	2.07	1.46	7.78	0.76
6^+	18.21	0.035	67.3	17.83	0.72	1.19	2.07	1.46	7.78	0.76
8^+	19.84	0.035	67.3	19.21	0.72	1.19	2.07	1.46	7.78	0.76
10^+	21.73	0.035	67.3	20.85	0.72	1.19	2.07	1.46	7.78	0.76
12^+	23.80	0.035	67.3	22.71	0.72	1.19	2.07	1.46	7.78	0.76
14^+	26.02	0.035	67.3	24.77	0.72	1.19	2.07	1.46	7.78	0.76

The PHFB as well as the VAP results in ^{102}Pd. For further comments see Table IV.1

		VAP								
J^π	E_J(PHFB)	β_J	$\langle \phi(\beta_J) \lvert Q_0^2 \rvert \Phi(\beta_J) \rangle$	E_J(VAP)	Occupation Probabilities(Neutrons) 1/2	3/2	5/2	7/2	9/2	11/2
0^+	24.61	0.00	66.3	24.61	0.72	1.29	2.30	1.60	8.55	1.51
2^+	24.96	0.00	66.3	24.96	0.72	1.29	2.30	1.60	8.55	1.51
4^+	25.72	0.00	66.3	25.72	0.72	1.29	2.30	1.60	8.55	1.51
6^+	26.83	0.035	79.1	26.60	0.75	1.36	2.20	1.90	7.67	2.11
8^+	28.21	0.07	81.1	27.72	0.77	1.37	2.17	1.98	7.57	2.14
10^+	29.80	0.07	81.1	29.01	0.77	1.37	2.17	1.98	7.57	2.14
12^+	31.57	0.07	81.1	30.48	0.77	1.37	2.17	1.98	7.57	2.14
14^+	33.46	0.07	81.1	32.09	0.77	1.37	2.17	1.98	7.57	2.14

In figure 8 we present a comparison of the VAP and the observed spectra in ^{100,102}Pd. Here we notice that the observed level spacings in the lower part of the yrast cascade (with J=0 through 8) are reasonably well reproduced by the present calculation for these nuclei. In ^{100}Pd, however, the positions of the calculated yrast states with J=10 and 12 are about 1.5 MeV too high compared with the experiments. In the nucleus ^{102}Pd the computed position of the J=12 level shows a discrepancy of about 1.3 MeV.

We have indicated in figure 8 some of the observed, high-spin yrare levels in ^{100,102}Pd. The figure also shows the positions of these yrare levels calculated by carrying out angular momentum projection on the intrinsic HFB state. The PHFB states are seen to be in poor agreement with the observed yrare levels. The results thus indicate that the mixing of the K=0 HFB intrinsic states with other high-lying (quasiparticle-excited) K=0 bands may be quite significant from the point of view of an accurate description of the high-spin yrare levels in ^{100,102}Pd.

In tables IV.3 and IV.4 we have given the reduced transition probabilities for electric quadrupole transitions, B(E2), as well as the static quadrupole moments for the yrast cascades in ^{100,102}Pd.

A comparison of the computed values of the electromagnetic observables with the experiments is expected to provide a sensitive check on the wavefunctions employed. However, a lack

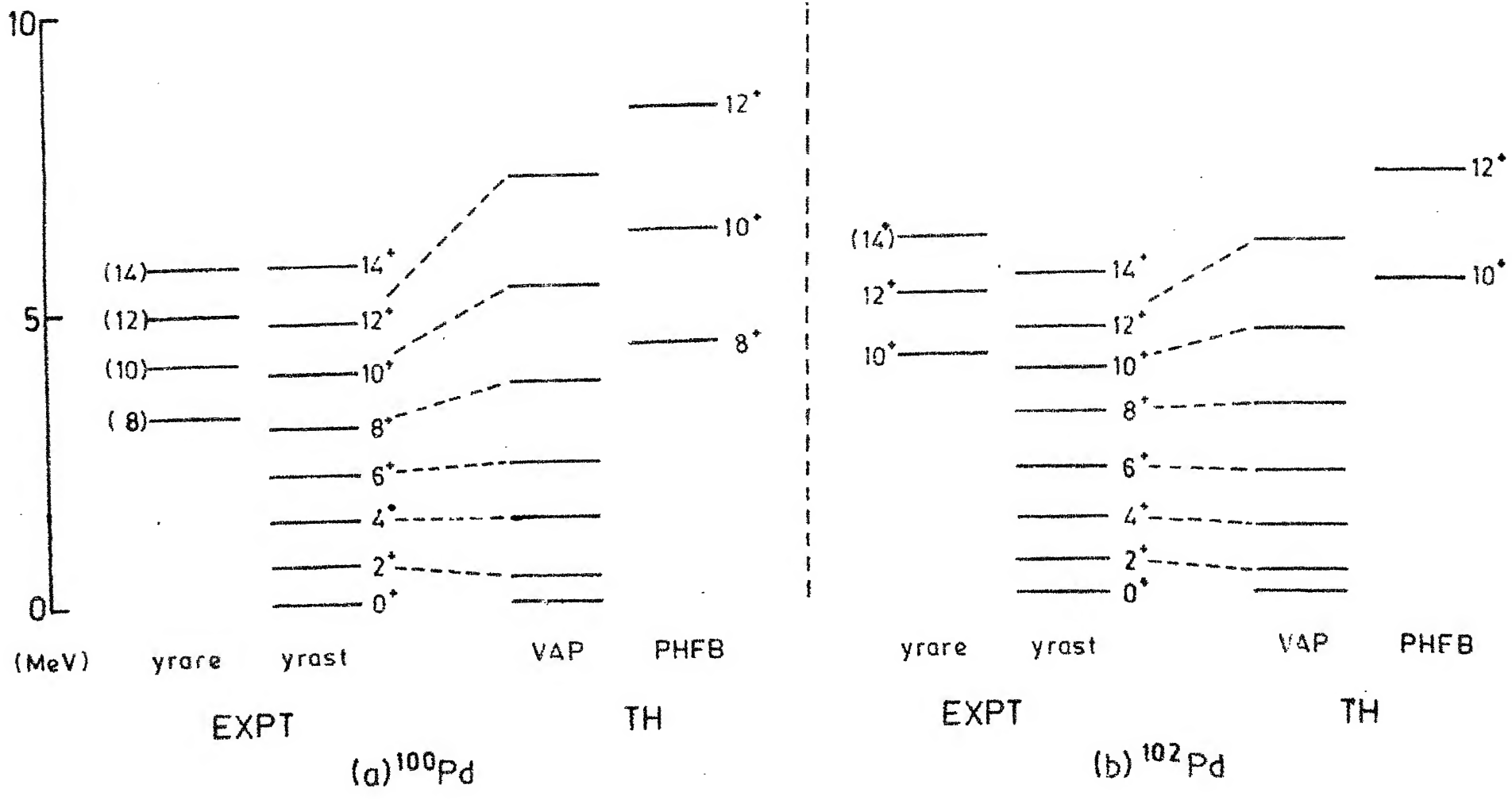

Fig. 8. Calculated (TH) and experimental (EXPT) levels in ^{100,102}Pd.

TABLE IV.3

The reduced transition probabilities for the electromagnetic E2 transitions as well as the static quadrupole moments for the yrast levels in ^{100}Pd. The reduced transition probabilities and the static moments have been given in units of $e^2.b^4$ and $e.b^2$ respectively, where b is the oscillator parameter. Here e_p (e_n) denotes the effective charge for protons (neutrons).

Transition $J_i^+ \rightarrow J_f^+$ $[E(J_f^+)-E(J_i^+)]$ in KeV	$[B(E2)]^{1/2}$	$Q(J_f^+)$
$0^+ \rightarrow 2^+$ (665.3)	$10.75\ e_p + 13.91\ e_n$	$-6.86\ e_p - 8.88\ e_n$
$2^+ \rightarrow 4^+$ (750.5)	$6.51\ e_p + 9.53\ e_n$	$-8.88\ e_p - 13.12\ e_n$
$4^+ \rightarrow 6^+$ (773.0)	$15.66\ e_p + 22.75\ e_n$	$-11.23\ e_p - 16.24\ e_n$
$6^+ \rightarrow 8^+$ (798.6)	$16.03\ e_p + 23.28\ e_n$	$-11.88\ e_p - 17.12\ e_n$
$8^+ \rightarrow 10^+$ (881.4)	$16.23\ e_p + 23.57\ e_n$	$-12.34\ e_p - 17.70\ e_n$
$10^+ \rightarrow 12^+$ (892.0)	$16.35\ e_p + 23.75\ e_n$	$-12.69\ e_p - 18.11\ e_n$
$12^+ \rightarrow 14^+$ (945.4)	$16.39\ e_p + 23.35\ e_n$	$-12.98\ e_p - 18.42\ e_n$

TABLE IV.4

The results for the reduced transition probabilities as well as the static quadrupole moments for the yrast levels in ^{102}Pd

Transition $J_i^+ \rightarrow J_f^+$ $[E(J_f^+)-E(J_i^+)]$ in KeV	$[B(E2)]^{1/2}$	$Q(J_f^+)$
$0^+ \rightarrow 2^+$ (556.4)	12.19 e_p + 18.01 e_n	-7.79 e_p-11.57 e_n
$2^+ \rightarrow 4^+$ (719.3)	14.57 e_p + 21.69 e_n	-9.94 e_p-14.73 e_n
$4^+ \rightarrow 6^+$ (835.5)	6.17 e_p + 8.35 e_n	-12.72 e_p-18.16 e_n
$6^+ \rightarrow 8^+$ (901.4)	19.09 e_p + 27.76 e_n	-14.19 e_p-20.29 e_n
$8^+ \rightarrow 10^+$ (714.6)	19.19 e_p + 28.09 e_n	-14.65 e_p-20.90 e_n
$10^+ \rightarrow 12^+$ (704.8)	19.17 e_p + 28.28 e_n	-14.96 e_p-21.36 e_n
$12^+ \rightarrow 14^+$ (892.4)	19.07 e_p + 28.38 e_n	-15.19 e_p-21.61 e_n

of availability of the yrast life-times in ^{100,102}Pd has prevented us from testing the VAP wavefunctions obtained in the present calculation.

We have noted earlier the significant increase in the deformations of the intrinsic states at the J=4 and J=6 yrast levels in ^{100,102}Pd respectively. From the B(E2) results presented in the tables IV.3 and IV.4 we find that these changes in the intrinsic deformations manifest themselves here in terms of sizable reductions in the $B(E2)(2^+ \rightarrow 4^+)$ and $B(E2)(4^+ \rightarrow 6^+)$ values in ^{100,102}Pd respectively.

A measurement of the yrast half-lives in ^{100,102}Pd would not only be interesting in itself, it would also help establish the band parentage of the various yrast levels in these nuclei.

IV.4 Conclusions

Summing up, the present VAP calculations for the low-lying levels in ^{100,102}Pd are fairly successful in explaining, in a microscopic manner, the significant departures from the rotational behaviour that characterize the observed yrast spectra in these nuclei.

The results presented here reveal that the increase in the intrinsic deformations of the yrast levels (with $J \geq 2$) in ^{100,102}Pd is due to the enhanced occupation of the $1h_{11/2}$ orbit. In other words, the observed "centrifugal stretching" in ^{100,102}Pd is due to a selective participation of the $1h_{11/2}$ orbit for some of the yrast levels.

REFERENCES

1. G. Scharff-Goldhaber, M. McKeown, A.H. Lumpkin and W.F. Piel Jr., Phys. Letters 44B (1973) 416.

2. M.A.J. Mariscotti, G. Scharff-Goldhaber and B. Buck, Phys. Rev. 178 (1969) 1864.

3. B.C. Smith and A.B. Volkov, Phys. Letters 47B (1973) 193.

4. L. Satpathy and S.C.K. Nair, Phys. Letters 26B (1968) 257, R. Dreizler, P. Federman, B. Giraud and E. Osnes, Nucl. Phys. A113 (1968) 145;
   J. Vojtik, Nucl. Phys. A212 (1973) 138;
   E. Caurier and B. Grammaticos, Nucl. Phys. A279 (1977) 333.

5. N. Onishi and S. Yoshida, Nucl. Phys. 80 (1966) 367.

6. L. Hasselgren, C. Fahlander, J.E. Thun, B. Orre and N.G. Jonsson, UUIP-957 (1977);
   L. Hasselgren, in Interacting Bosons in Nuclear Physics, edited by F. Iachello (Plenum Press, New York and London, 1979), p 67.

CHAPTER V

CONCLUSIONS

Looking through the chart of the nuclides one comes across an interesting region between A=90 and A=110. In this region one encounters at one end classic shell-model nuclei such as ^{90}Zr and ^{92}Mo and, at the other end, classic rotors like ^{102}Zr, ^{104}Mo and ^{106}Mo. The present study was motivated by a desire to gain some insight into this phase-transition from spherical to deformed nuclei.

Our HF-oriented study of the effective interactions operative in the 2s-1d, 2p-1f and 2p-1f-1g shells provided a qualitative understanding of the occurrence of deformations in the Zirconium region. An important spin-off of this study was the result that the relative importance of the pairing correlations in the like-particle and the neutron-proton channels depends very much on the spectrum of the spherical single-particle energies. An appreciation of this role of the single-particle energies turns out to be instrumental in understanding the absence of rotational features in the N>Z nuclei in the 2s-1d and 2p-1f shells.

In chapters III and IV we have focussed our attention on the quantitative description of the quasirotational yrast spectra in some doubly-even Zirconium, Molybdenum and Palladium isotopes, employing the CHFB and the VAP techniques in

conjunction with the pairing-plus-quadrupole-quadrupole effective interaction. The calculations indicate that the origin of the sudden onset of large deformations in the highly neutron-rich isotopes of the Zirconium and Molybdenum can be traced back to the involvement of the $1h_{11/2}$ orbit in the underlying configuration space. The observed centrifugal stretching in the nuclei ^{100,102}Pd is also found to be connected with an enhancement of the $1h_{11/2}$ occupation (for neutrons) in the $J \geq 2$ states of the yrast bands.

The present study was concerned primarily with the rotational features in the available yrast spectra with $J \leq 8$ in the Zirconium region; we did not examine the high-spin spectra in this region. The calculations presented here have revealed that the time-reversed pairs of $1h_{11/2}$ neutrons are just below the relevant Fermi surfaces in the Zirconium and Molybdenum isotopes. Therefore, at higher excitation energies, the orbit $1h_{11/2}$ is likely to play a role somewhat akin to that played by $1i_{13/2}$ orbit in the rare-earth region where it leads to backbending effect through a realignment of the $1i_{13/2}$ pair. It will thus be very interesting to study the high-spin yrast spectra in the Zirconium region, both from theoretical as well as experimental point of view.